Department of Physics and Astronomy
Heidelberg University

Bachelor Thesis in Physics
submitted by

Julius Vincent Dehne

born in Gießen (Germany)

2023

Stage-static and Laser-static Out-of-Plane Setups for Switching Phase Change Materials

This Bachelor Thesis has been carried out by Julius Dehne at the
Kirchhoff Institute for Physics in Heidelberg
under the supervision of
Prof. Dr. Wolfram Pernice

Abstract

The increasing demand for fast and energy-efficient processing units, especially for the application in the field of artificial intelligence or more concretely neural networks take electrical processing units to their limit. The usage of photonic integrated circuits could help to satisfy this demand. One solution is the application of phase-change materials as weights in a matrix tensor core. To switch the phase of these weights different approaches can be used.

In this thesis two out-of-plane optical setups connected with an ultrashort pulsing laser are built, compared and used for switching. The Stage-static setup with a 10x objective offers the biggest movement area of $(1550 \pm 40)\mu\text{m} \times (1560 \pm 40)\mu\text{m}$ with low power fluctuations, while the Laser-static setup has no power fluctuations but a smaller movement area. The resolution is equal for both setups and is $(1.6 \pm 0.2)\mu\text{m}$ for the 10x objective and $(0.8 \pm 0.1)\mu\text{m}$ for the 50x objective.

These setups are used for amorphization of crystalline Ge-Sb-Te (GST). This was only achieved accidentally and was not reproducible due to possible oxidation and possibly a too high repetition rate of the laser pulses.

Zusammenfassung

Der stetig steigende Bedarf an schnellen und energieeffizienten Prozessoren, insbesondere für die Anwendung im Bereich der künstlichen Intelligenz oder genauer der neuronalen Netzwerke, bringt elektrische Prozessoren an ihre Grenzen. Der Einsatz photonischer integrierter Schaltkreise könnte diese Nachfrage zu befriedigen. Eine Lösung basiert ist die verwendung von Phasen wechselnden Materialien als Gewichte in einem Matrix-Tensor-Kern. Zum Ändern der Phase dieser Gewichte können verschiedene Ansätze verwendet werden.

In dieser Arbeit werden zwei optische out-of-plane Aufbauten, die mit einem ultrakurz gepulsten Laser verwunden sind, gebaut, verglichen und zur Änderung der Phase verwendet. Der Stage-static Aufbau mit einem 10x Objektiv bietet den größten Bewegungsbereich von $(1550 \pm 40)\mu\text{m} \times (1560 \pm 40)\mu\text{m}$ bei geringen Leistungsschwankungen, während der Laser-static Aufbau keine Leistungsschwankungen, aber einen kleineren Bewegungsbereich aufweist. Die Auflösung ist bei beiden Aufbauten gleich und beträgt $(1,6 \pm 0,2)\mu\text{m}$ für das 10x-Objektiv und $(0,8 \pm 0,1)\mu\text{m}$ für das 50x-Objektiv.

Diese Aufbauten werden für die Amorphisierung von kristallinem Ge-Sb-Te (GST) verwendet. Dies wurde nur unabsichtlich erreicht und war aufgrund möglicher Oxidation und möglicherweise zu hohen Frequenz der Laserpulse nicht reproduzierbar.

Contents

1 Introduction

Artificial Intelligence (AI) is nowadays a highly discussed topic. The reason for this is the huge development of generative AI in the last year, which can be used for good or bad purposes. A few examples of generative AI are ChatGPT, Stable Diffusion, Soundify and Codex, all published in 2022 [1]. They all have in common that they can generate new content from an input text, like texts, images, videos or code. As already mentioned, such a potential can be used for bad purposes, like for example generating fake news. At the moment, the EU is the first institution to regulate its usage by law through the so called AI Act [2].
Other important examples of AI are the computer program "Watson", developed by IBM, winning the quiz show "Jeopardy!" in the year 2011 [3] or "AlphaGo", developed by Google DeepMind winning the strategy board games "Go" against the best "Go" player in 2016 [4], showing the huge potential of AI. There are also other applications which are not as obvious in the first moment like face-recognition or autonomous driving [5].
All these applications have as common ground that a huge amount of data has to be processed [6]. To deal with this, the size of transistors in integrated electronic circuits has to go down further and further. This evolution can still be described with Moore's law, stating that the number of transistors on a single chip doubles every two years. However already a trend is visible that the evolution cannot keep up with the law anymore [7].
One idea to challenge these problems is to use photonic integrated circuits (PIC). They offer the ability for parallel processing, done with wavelength multiplexing and optical frequency combs, so that multiple sets of data can pass through the circuit at the same time. Like this, it is possible to work with a huge amount of data [8].
For multiple applications where multiply and accumulate operations are needed, a photonic tensor core can be used. The working principle is based on a vector matrix multiplication and is shown in Figure 1.1. The matrix elements or weights are represented by a phase-change material cell placed on top of waveguides. These cells can reduce the transmitted light dependent on its phase. Since there are not only the two states in which all light is transmitted or absorbed, but also intermediate ones, the core can work in another numeral system than the dual one. The values of the vector are given by the amplitude of the laser pulses sent into the waveguides. The initial laser pulses are modified by the phase-change material cell and then added together to form the result vector, so that a

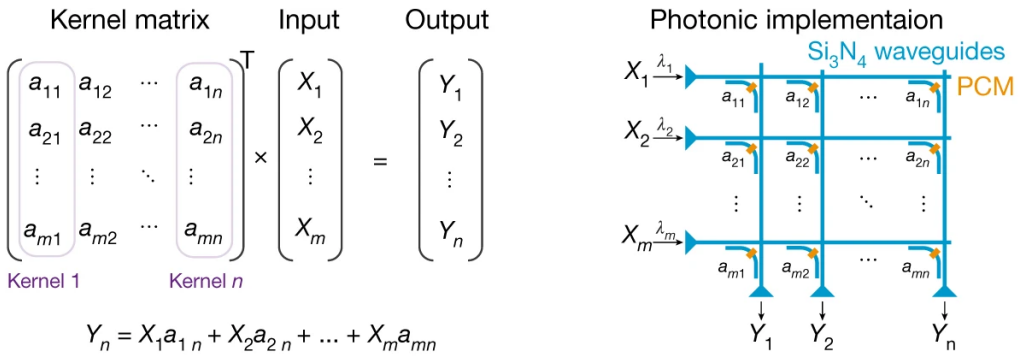

Figure 1.1: On the left side, the theoretical matrix multiplication is shown and on the right side, a photonic matrix tensor core. From the left the input vector is sent into the matrix and at the bottom the output vector can be measured. The weights or the matrix elements are represented by phase-change material (PCM) cells at the crossing point of the waveguides in horizontal and vertical direction [8].

matrix multiplication is directly realised in one step and not in a series of single steps like it is done within conventional computers [8].
Switching these matrix weights is one of the crucial steps. It can be done electrically with current pulses or optically with laser pulses. Since a solution based on direct connection on the chip, either electrical or optical ones, is quite space consuming, other solutions are of interest. This thesis focuses on a solution based on a free space laser beam hitting and there by changing the phase-change material.
The first part gives a short introduction into the physics of phase-change materials, with a special focus on the one used in this thesis. In the next section, two different setups for switching are compared. Therefore, first the construction and design is explained, including all the necessary components and followed by an evaluation based on different criteria to find the most suitable setup. In the last part, the setups are used to finally study the behavior of a phase-change material if hit with a laser with the goal of being able to control the setups in such a way that reversible switching is repeatedly possible so that it can be used for phase-change material cells on waveguides to study their behaviour there.

2 Phase-Change Materials

A variety of different types of phase-change materials (PCMs) exists. In this thesis, solid-solid PCMs are used, which can transition between an amorphous and a crystalline state [9]. These two states differ in their atomic bounds. The amorphous state is built out of covalent bounds and has no long-range order, while the crystalline state is dominated by resonant bounds with long-range order [10]. These different bounds influence significantly the optical and electrical properties of the PCM.
In the covalent bounds the electrons are strongly localized leading to a low conductivity and therefore to a high resistance. In the resonant bounds the electrons are highly delocalized, which goes together with a high conductivity and a low resistance.
Similar argumentation can be done based on the stoichiometry leading to a great difference in the refractive index [10][11][12].
Since the PCM is used to change the transmission of light, the main interest lies in the optical contrast, that means the difference between the refractive indices. It is expected that the crystalline state has a higher absorption coefficient than the amorphous state [10][12].
To change from the phase of a PCM from the crystalline state to the amorphous one it has to be heated up above the melting temperature and cooled down quickly, so that no crystals can be formed. To switch then back to the crystalline state the PCM has to be heated up between the melting and the glass temperature, which is the temperature where the solid turns into a viscous liquid. Afterwards the PCM is cooled down, so that crystals are formed [9]. This switching process can be seen in Figure 2.1. In red the amorphization process of a PCM is shown and in blue the crystallization process.

To heat the PCM up sufficient power is required. This can be done either electrically or optically. To switch the PCM electrically some conducting connections are needed and therefore the production of a chip with optical and electrical components is more complicated than the one only with optical components. For optical switching, short laser pulses are used, connected through waveguides directly on the chip. This is called in-plane switching. However the problem is the amount of space needed for these additional waveguides. Here the variant of out-of-plane switching has its benefits, by using a free space laser which is focused on the cell.

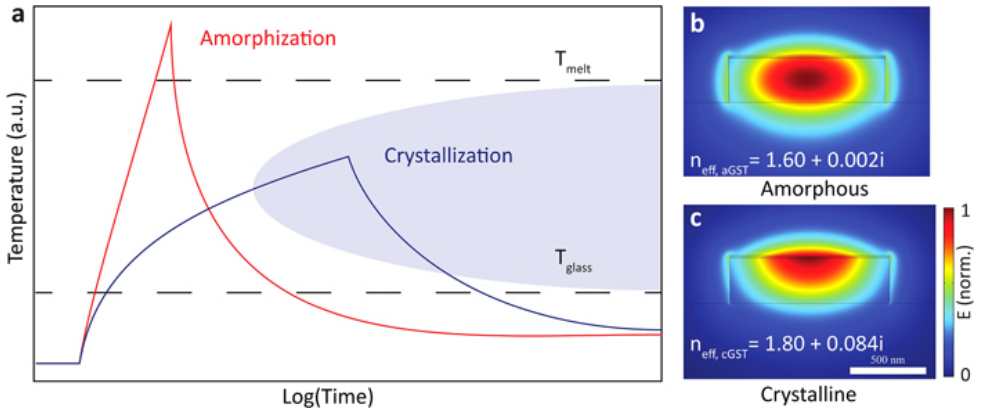

Figure 2.1: The diagramm shows the different processes for crystallization and amorphization. On the right side simulations for the optical mode profiles for a silicon nitride waveguide with a PCM on top are shown. Due to the phase of the PCM the refractive index changes of the guided modes within the waveguide[10].

One well studied PCM is the chalcogenide $Ge_2Sb_2Te_5$ (GST), based on the germanium (Ge)–antimony (Sb)–tellurium (Te) alloys [13]. This PCM is also used for this thesis. It offers a high optical contrast between the two different states and can be changed rapidly in the timescale of ns [14].

In this thesis the out-of-plane switching method is used to switch crystalline GST to the amorphous state. Switching back to the crystalline state is done by heating the whole chip up with a hotplate and let it cool down. In this way, the PCM can recrystallize again. It is also possible to use a laser for this, but then the duration of the pulses should be changeable. In this case the switching back is only possible with the hotplate, since the duration of the pulses of the used laser cannot be adapted.

3 Experimental Setups

As described, PCM need to be heated up to be switched. In order to only switch between the states and not burn the material the energy has to be controllable. Since the goal is to switch many PCM cells on a chip, either the spot of the focused laser or the chip itself should be movable. These two possible setups are called Stage-static setup or Laser-static setup. The setups are based on the ideas of a Laser-scanning-microscope and a Probe-scanning-microscope, respectively and are then adapted here to be suitable for switching the phases. The Stage-static and the Laser-static setups are compared to find out, which one is more suitable for the given application. Mainly four different criteria are compared: the movement area, the power fluctuations within the movement area, the resolution and the movement speed.

3.1 Laser-setup

The first part of the whole setup is the Laser-setup (see Figure 3.1). It contains the Mai-Tai Laser (Mai-Tai HP [15]), generating laser pulses of $\Delta t = 100\,\text{fs}$ duration with a repetition rate of $r_0 = (80 \pm 1)\text{MHz}$. It was planned that the next component in the light path would be the pulse-picker (UHG-PSK [16]), but unfortunately the main component, the Bragg-cell, was defect and the diagnosis and the repair took such a long time, that it was not possible to use it in the time of this Bachelor thesis. As the name already suggests, it could have selected some of the laser pulses and therefore reduce the repetition rate. The next main component is the attenuator (VA-BB-2 [17]). The working principle is that a $\lambda/2$-waveplate is rotated by an angle α in front of a Glan-laser polarizer. This then leads to a relative polarization angle of 2α between the laser and the polarizer and a reduction of the power. The resulting power can be derived by Malus's law [18]:

$$P(2\alpha) = P_0 \cos^2(2\alpha) = \frac{P_0}{2}\cos(4\alpha) + \frac{P_0}{2} \tag{3.1}$$

with P_0 as the maximal power.

Since the two setups are compared and additionally one of them is standing on an extra table, it would be difficult to connect the Laser-setup with the Stage-static and Laser-static one by only using mirrors. To make it easier, an optical fiber is used as a connection. To get the laser light into the optical fiber a collimator (FiberPort Collimator [19]) is

needed to focus the light into the core of the optical fiber. There exists a wide variety of collimators with different properties. The one used here is not the best for this application since it is optimized for bigger beam sizes than the Mai-Tai laser emits. To solve this, two lenses (AC254-075-B-ML - $f = 75$mm [20] and AC254-200-B-ML - $f = 200$mm [21]) are used to magnify the beam size by 2.654 times from 1.2mm to 3.1848mm. That way, the transmission could already be increased. For further increasement, two adjustable mirrors [22] were used to align the beam even more properly and are also used to direct the laser around the pulse-picker.

One main problem which occurred in this setup is that there are some back reflections propagating into the Mai-Tai laser. This causes the laser to stop pulsing or even the power is reduced significantly. An attempt to solve this problem was placing all the components slightly angled. This solution did not work out, because the problematic back reflection is coming from the end of the optical fiber which should not be placed angled since the transmission is highly reduced in that position. So the next attempt was using an additional polarizer ([23]) and a $\lambda/4$ wave-plate so that the initial light has a different polarization then the reflected light. In this way, the reflected light should be filtered out. This works partially, as the angle of the attanuator can be rotated only in a small range around the minimum, otherwise the back reflection were still too strong, causing the laser to stop pulsing. Even though, the power of the pulsed laser beam was now strong enough to burn the PCM and therefore no further optimization was done.

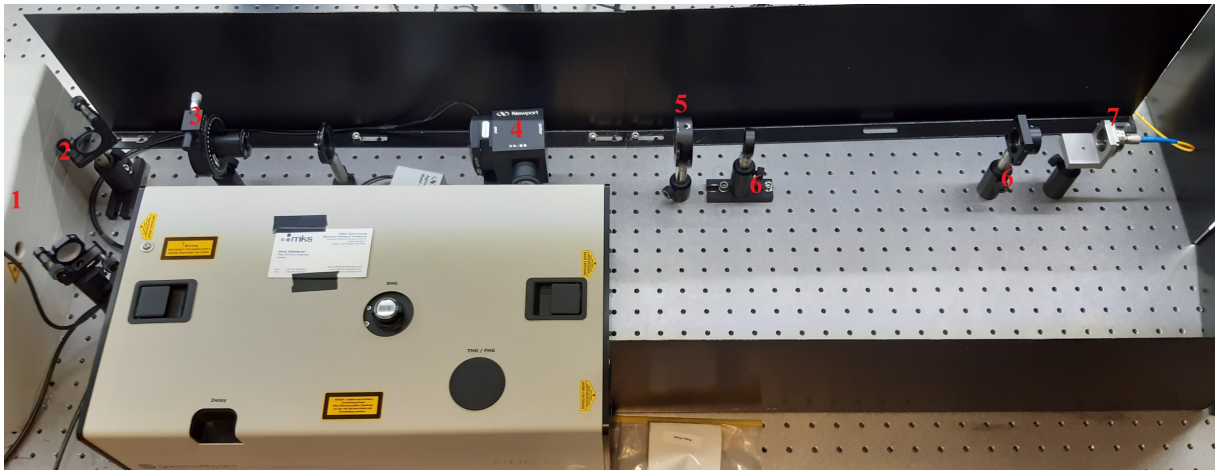

Figure 3.1: In the Laser-setup the light exits the Mai-Tai laser (1), is then aligned with the two mirrors (2) to pass through the additional polarizer (3), the attenuator (4), the $\lambda/4$ wave-plate (5) and the magnifying lens system (6). At the end of the setup the laser beam is coupled with the collimator (7) into an optical fiber. The gray box at the bottom of the picture is the pulse-picker, which was not included in the optical path due to its defect.

Since the Mai-Tai Laser is generating pulsed laser beams the peak power can be calculated with the average power P, the repetition rate r and the pulse duration Δt:

$$P_{Peak} = \frac{P}{r \cdot \Delta t} \tag{3.2}$$

3.2 Stage-static setup

The first setup is the Stage-static one, here the probe or chip is fixed in its position and the focus point of the laser is moving. To achieve this, an optical setup is needed, embedded into a fixed Thorlabs Cage System [24]. A sketch of the setup is given in Figure 3.2 and a picture in Figure 3.4. The idea of the setup is based on the one found in the Bachelor

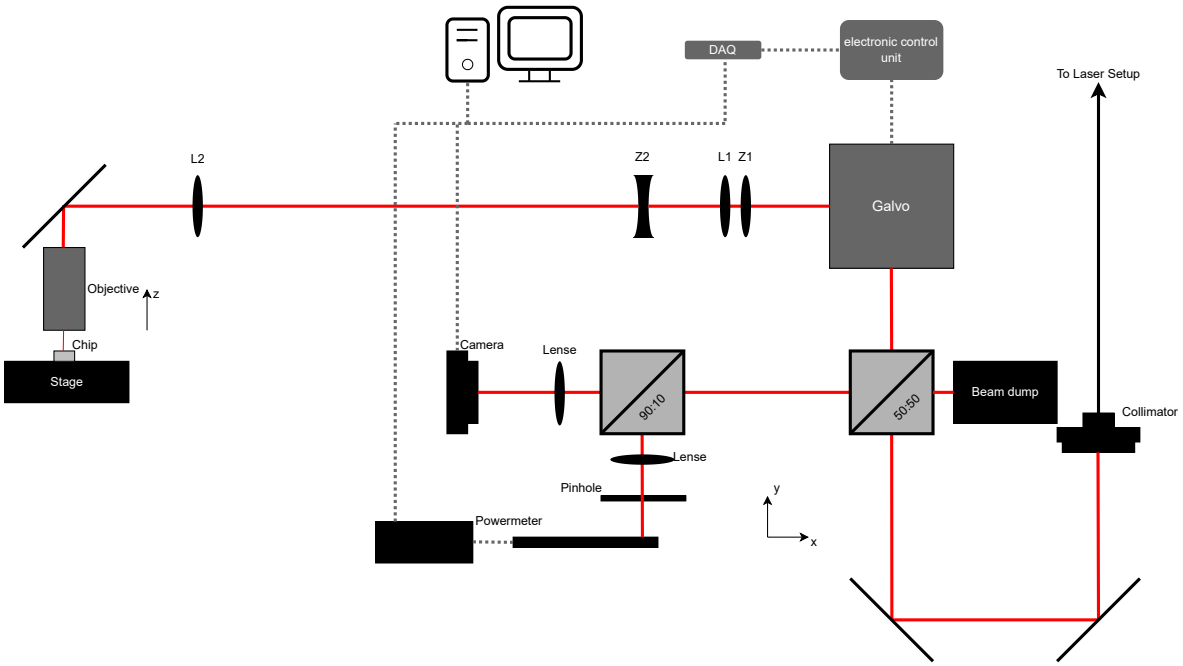

Figure 3.2: Detailed sketch of the LSM setup: All the main components are shown and the path of the laser is drawn in red.

Thesis of Niklas Hesse [25] and Björn Luig [26] and is adapted with help of the Bachelor Thesis of Robert Schneider [27].
The laser light exits the optical fiber with the help of a collimator [28]. From there, two mirrors [22] are used to align the laser into the Cage System. The beam then hits a beam splitter [29] with a ratio of 50:50. 50% of the beam goes directly into a beam trap [30], the other 50% goes to the main component of the setup: the 2D Galvanometer System [31]. It contains two mirrors which can be independently rotated by applying a voltage to the electronic control unit [32]. This voltage is controlled by a PC with the help of a data acquisition unit (DAQ) [33]. The mirrors can be rotated by $\pm 10°$ to the optical axis.

After the Galvo a telecentric lens system follows with two cylindrical lenses. From there, the beam hits another mirror and is then focused with a 50x objective [34] or a 10x objective [35] onto the chip. The chip itself is laying on a movable stage, especially the z direction is quite important to move the chip into the focus point of the objective. This is easier than moving the objective itself since all the distance between the lenses and the objectives should stay fixed.

3.2.1 Telecentric lens system

With the telecentric lens system the possible movement area on the chip should be extended, because the back focal plane of the objective is only a few millimeters away from the objective and should be at the position of the moving mirrors. Due to the geometrical dimensions of the different components this is not possible, so some movement area is lost in this direct setup. With a telecentric lens system the back focal plane is projected onto the moving mirrors. Another problem is that the objective can only handle a beam with an angle smaller than the $\pm 10°$. Here also the telecentric lens system helps by translating bigger angles into smaller ones as illustrated in Figure 3.3.

$$\frac{\alpha}{\beta} = \frac{f_{L2}}{f_{L1}} \tag{3.3}$$

Due to the lenses the beam size is increasing as well:

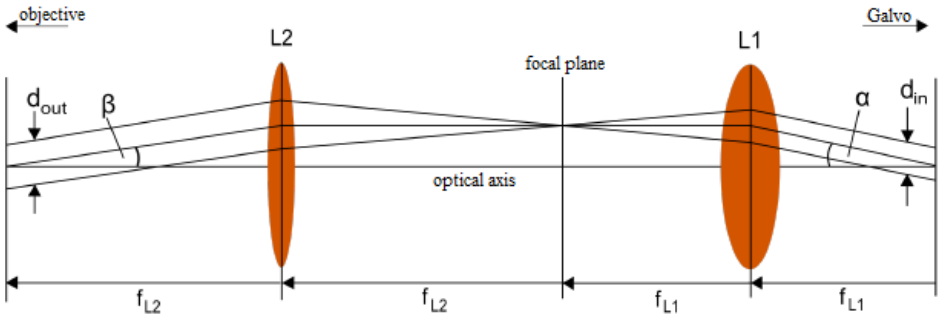

Figure 3.3: The working principle of the telecentric lens system is illustrated. On the right side would be the Galvo and on the left the objective would follow (adapted from the [27]).

$$\frac{d_{out}}{d_{in}} = \frac{f_{L2}}{f_{L1}} \tag{3.4}$$

Since the two moving mirrors of the Galvo are not at the same position, it is not possible to project the back focal plane on both of them. Therefore, another correction is needed. For that, two cylindrical lenses are used, which only affect the light in one axis and thereby make it possible to project the back focal plane onto the respective two moving mirrors.

The values of the lenses (see Table 3.1) and also their positions are taken from the Bachelor Thesis of Robert Schneider and are also aligned in the way he described [27].

	Z1 [36]	L1 [20]	Z2 [37]	L2 [21]
f [mm]	1000	75	-400	200

Table 3.1: Lenses used in the telecentric lens system

With these lenses a translation of the angles and an enlargement of the beam size of 2.654 is achieved. This results in a theoretical maximum angle for the Galvo of 5.34° [27].

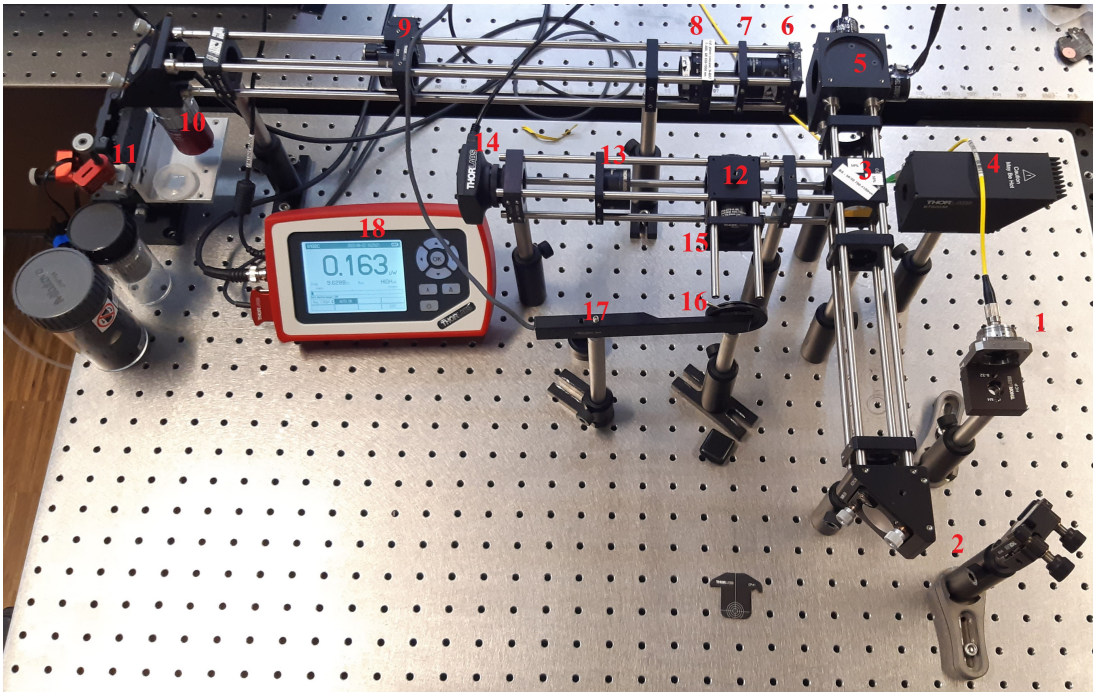

Figure 3.4: The laser beam is exiting the optical fiber at the collimator (1) and is then aligned with two mirrors (2) into the cage system. The 50:50 beam splitter (3) splits the light in the direction of the beam trap (4) and the Galvo (5). From the Galvo the beam passes through the first cylindrical lens (6), then the first telecentric lens (7), followed by the second cylindrical lens (8) and the second telectentric lens (9). Afterwards follows the objective (10), which focuses the light onto a chip lying on the stage (11). For the detection, the light is reflected back from the chip until the first beam splitter, from there it goes to the 90:10 beam splitter (12). This divides the light in the direction of the camera (14) with a lens (13) in front and in the direction of the power meter (17 and 18), also with a lens (15) and a pinhole (16) in front.

3.2.2 Detection

Previously described was only one direction of light travelling trough the setup. The setup can also be used to get an image of the chip. Therefore the reflected light from the chip is going back through the telecentric lens system and is reflected by the Galvo to the beam splitter. Now 50% of the beam goes to another beam splitter [38]. There, 10% are focused with a lens [39] on a camera [40] and the other 90% are focused with a lens [41] through a pinhole [42] to a power detector [43][44]. The camera was only used for alignment, since no white light source is connected. Therefore, only one spot of the chip is reflecting, which can then be seen on the camera. For the image taking process the path with the power meter is used. The setup, as described, works as a confocal microscope. To get an image, the chip is scanned by moving the Galvo, the reflected power is measured and afterwards an image is reconstructed out of the data.

3.3 Laser-static setup

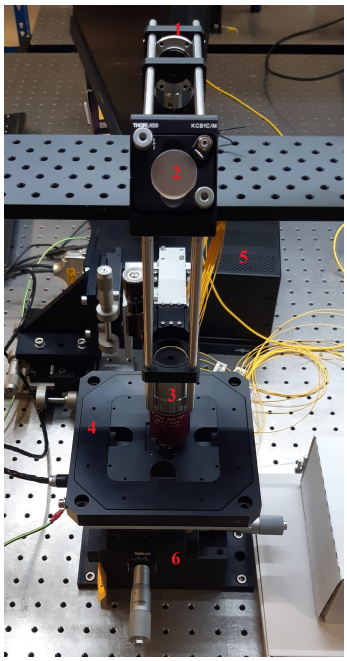

Figure 3.5: The light exits the optical fiber at the collimator (1), is then guided with a mirror (2) into the objective (3). Underneath is the piezo moving stage (4) connected with the electronics (5). Since the range of the piezo stage is small it is mounted on top of another stage (6), which is movable manually.

The second setup is the Laser-static one, where the stage holding the chip is moving, while the laser remains static. It can be seen in Figure 3.5
A small optical path is also needed here, consisting of a collimator [28] for the laser exiting the optical fiber, a mirror [22] to align the light path and the 50x objective [34] or the 10x objective [35]. In this setup the main component is a Piezo Stage from Physik Instrumente [45]. With this stage it is possible to move the chip very fast and precisely in a small area. It is controlled by an electronic unit [46] and a given software by the manufacturer [47]. In this way, the laser stays static while the chip is moving underneath.

3.4 Comparison of the two setups

To find out which one of the two setups is more suitable, the earlier mentioned criteria are compared. To get a reference, a so called calibration chip is used. It contains multiple chessboard patterns in various known sizes (see Figure 3.6).

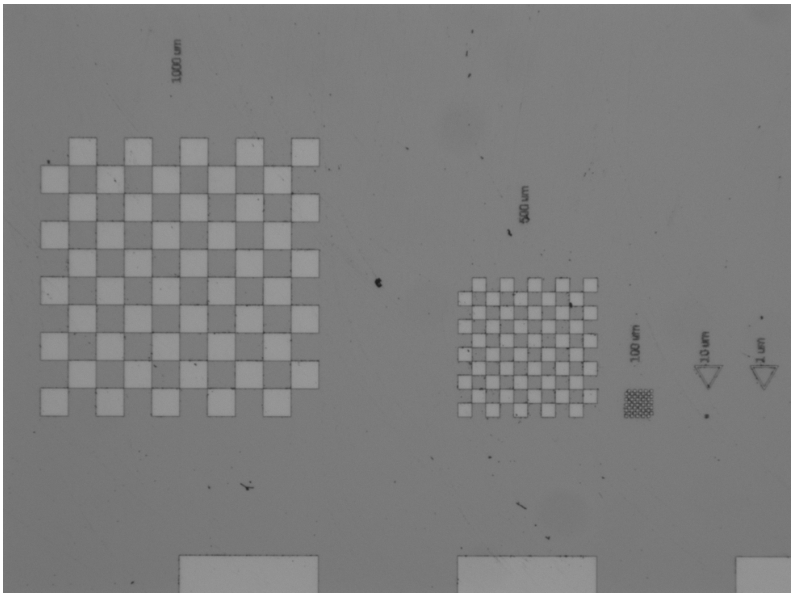

Figure 3.6: The calibration chip contains chessboard patterns with the sizes: $1000 \times 1000\mu$m, $500 \times 500\mu$m, $100 \times 100\mu$m, $10 \times 10\mu$m, $1 \times 1\mu$m and $5000 \times 5000\mu$m, shown only partially at the bottom of the image.

3.4.1 Movement area

The movement area of the Stage-static setup is investigated in two different ways, one by using it as a microscope and scanning the calibration chip and the other by burning GST on a chip by moving the Galvo between the maximum angles and measuring the area afterwards with another microscope. Both ways are also directly done with the two different objectives.

By choosing a suitable size of the chessboard pattern, the size of the scanning or movement area can be extrapolated (see Figure 3.7). For the 50x objective this gives a movement area of $(425 \pm 5)\mu$m in x direction and $(450 \pm 5)\mu$m in y direction and for the 10x objective $(2030 \pm 50)\mu$m in x direction and $(2160 \pm 50)\mu$m in y direction. In both scans it can be seen that the image is fading away, so there is no exact end of the picture. This and also the method of extrapolating is causing the uncertainties of the measurement.

The other way, burning the GST and measuring it afterwards, can be seen in Figure 3.8. Here the results for the movement area for the 50x objective are $(410 \pm 10)\mu$m in x direction and $(408 \pm 15)\mu$m in y direction and for the 10x objective $(1550 \pm 40)\mu$m in x

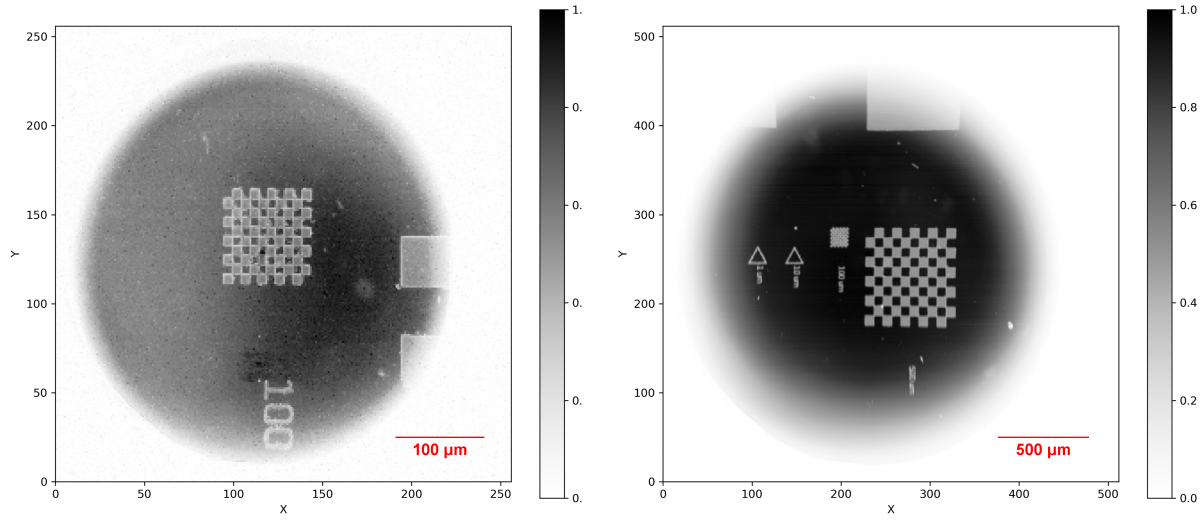

Figure 3.7: The calibration chip is scanned with the 50x objective, showing the 100 × 100μm pattern, (left image) and the 10x objective, showing mainly the 500 × 500μm at the center right, (right image).

direction and $(1560 \pm 40)\mu$m in y direction. Again it is visible that the lines fade away. The measurement is done by comparing the size of the structure with the chessboard patterns of the calibration chips by taking images with the same magnification. This leads to high uncertainties of the measurement.

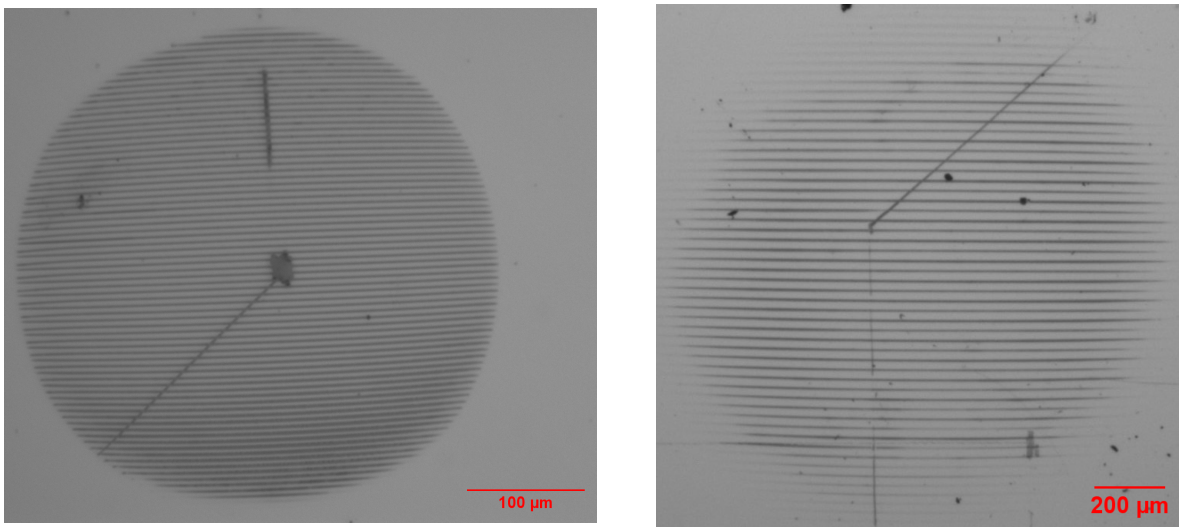

Figure 3.8: Multiple lines are burned into the GST with the 50x objective (left) and the 10x objective (right) and measured afterwards with another microscope.

By comparing the numbers it is obvious that the scanning area is bigger than the burning area. The explanation for this is that in the outer areas the power is no longer high

enough to burn the chip, because the beam is partially blocked by different components used in the setup.
These numbers can now be compared with the previous setups of Niklas Hesse, because one of the main goals of including the telecentric lens system in the setup presented in this thesis was to increase the possible movement area on the chip. Niklas Hesse got with his first setup a possible movement of $(400 \pm 50)\mu$m in x direction and $(680 \pm 50)\mu$m in y direction with the same 10x objective and with his last setup $(185 \pm 10)\mu$m in x direction and $(160 \pm 10)\mu$m in y direction with the same 50x objective [25]. This shows that with the help of the telecentric lens system the size of the possible movement area was increased by nearly three times. It is worth to mention that the number should not be taken too precisely since in Hesses's first setup he only measured the movement area with a camera and not by burning or switching a GST chip. Therefore, the burning of the GST chip is highly dependent on the used power, especially in the outer area.
With the setup of Robert Schneider, where the instructions for building the telecentric lens system came from, the measured values can not be compared since he used objectives with the same magnification but from a different manufacturer.

The movement area of the Laser-static setup is given by the movement area of the stage itself. The manufacturer Physik Instrumente states that it should be 200μm in both directions. Here also a chip completely covered with GST is used and is burned over the possible area and afterwards measured (see Figure 3.9). This gave a movement area of

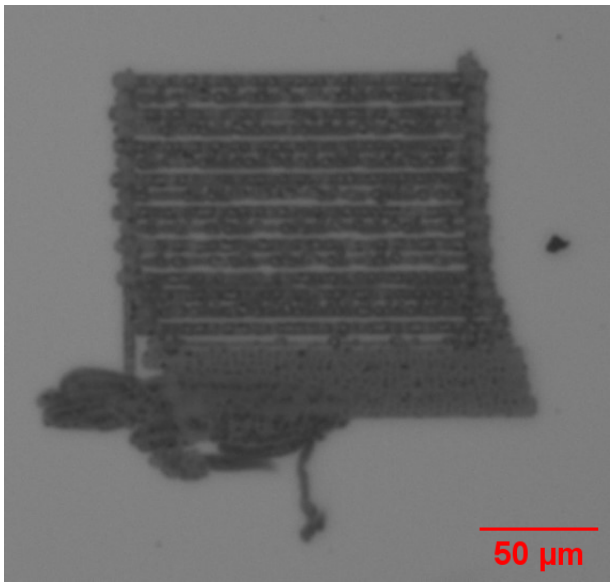

Figure 3.9: A rectangle is burned into a chip covered with GST and the size is measured.

$(140 \pm 5)\mu$m in x direction and $(150 \pm 5)\mu$m in y direction.
Interestingly, these measurements do not fit to the number given by the manufacturer. In

the bottom part of the rectangle the lines are moving to the right. The reason for this is that the stage was not fixed with screws at this moment and was therefore able to move a little bit. However, this does not explain the great differences in the movement area.
Due to the surprising result, the measurement was done multiple times, but the results were always the same: the measured movement area is smaller than the given value.

3.4.2 Power fluctuations within the Movement area

Due to the strong power dependency of the switching process, it is very important to know how much power is arriving at the chip at every position. In the Stage-static setup many components are changing the path of the laser beam, so it is interesting to see, whether this influences the power arriving at the chip.
To measure this, the power meter is placed directly on the stage instead of a chip and the Galvo is moved over the whole possible movement area. This measurement is done for both of the objectives. After the measurement the data is then reconstructed into an image (see Figure 3.10). The first impression is directly, that the power is not homoge-

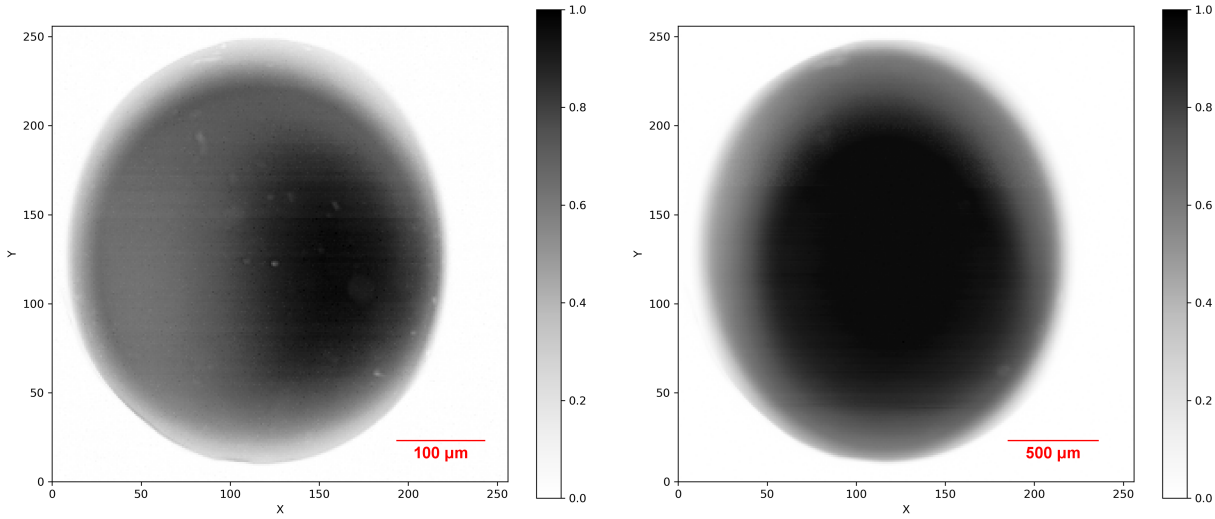

Figure 3.10: The relative power arriving at the chip with the 50x objective (left) and with the 10x objective (right) is measured with a power meter depending on the position of the Galvo.

neous distributed, especially for the 50x objective. The image of the 50x objective shows a huge problem, at about 25% of the area the full power is arriving and at 75% only 50% is arriving. Interestingly the area of full power is not circular shaped around the center point but mainly around a point in the right half. The image of the 10x objective shows an expected circular shape. In both images the power is reducing towards the outer part of the image.

The continuously reduced power at the edge of the circle can again be explained by the hitting of different components within the light path and therefore some parts of the beam are blocked. The unexpected shape of the image of the 50x objective could be explained with the much smaller entrance pupil of the objective. The telecentric lenses are increasing the beam to a size larger than the entrance pupil, therefore always some parts are blocked. Because of some small misalignment of the lenses this would lead to a significant difference in the final power fluctuations.
For the Laser-static setup no measurement was done, because the setup is constructed in such a way that the light path is static and nothing is moved in between, so that the whole area of movement the power reaching the chip is the same.

3.4.3 Resolution

The resolution can be defined in different ways, the one used here is based on the Rayleigh-criteria, stating that two point sources can still be distinguished if the maximum of one of the diffraction patterns is at the position of a minima of the other diffraction pattern [48]. Thus, to distinguish two structures with the microscope, the intensity of the light should drop recognizable in between.
Normally, the resolution is limited by the objective itself. In the data sheets of the objectives this value is already given, but to confirm this, some measurements are done. Especially for the ability of making images with the Stage-static setup it is interesting to see how much the additional optics influence the resolution and how small the structures can be to still be visible.
To measure the resolution, the calibration chip is scanned with the Stage-static setup with the two objectives (see Figure 3.11). This time, also the step size is reduced to a minimum (see Figure 3.12). In the next step, a GST chip is again used and the line size is measured to have a comparative value.

With both objectives, the smallest visible chessboard was the $10x10\mu$m one. By comparing the two images one can see that the 50x objective has a higher resolution than the 10x, because the arrows are displayed more sharply.
To exclude the influence of the step size, the area scanned on the chips is reduced to the chessboard pattern and the number of steps is increased so far that the smallest step size of the Galvo is reached (see Figure 3.12).

In the image no further structures are visible and it can be clearly seen that the stepsize is not the problem. Again, the difference between the two objectives can be seen, in the

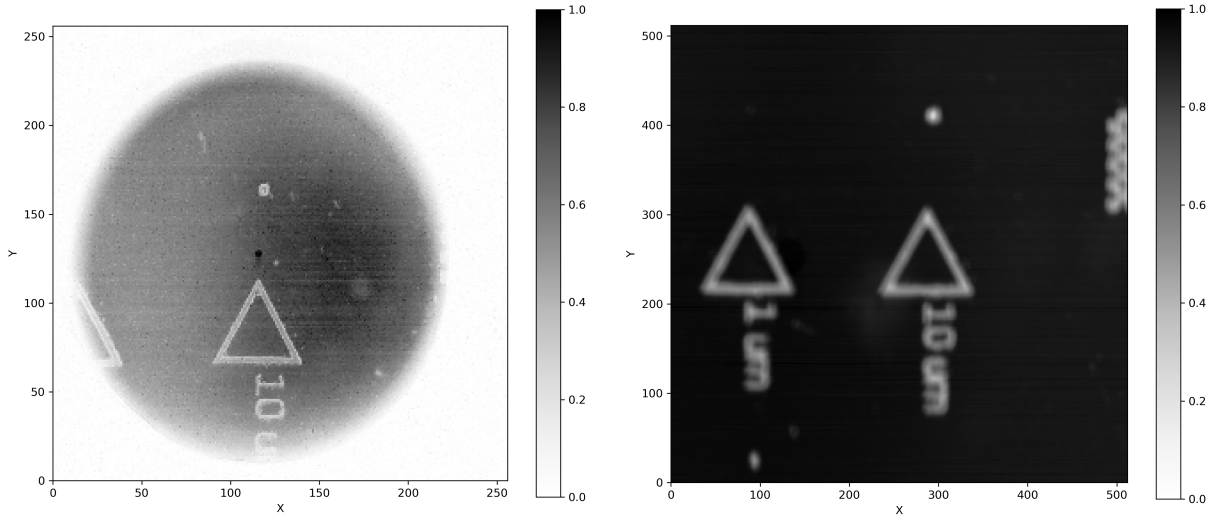

Figure 3.11: The $10 \times 10\mu$m chessboard is scanned with the 50x objective (left) and the 10x objective (right).

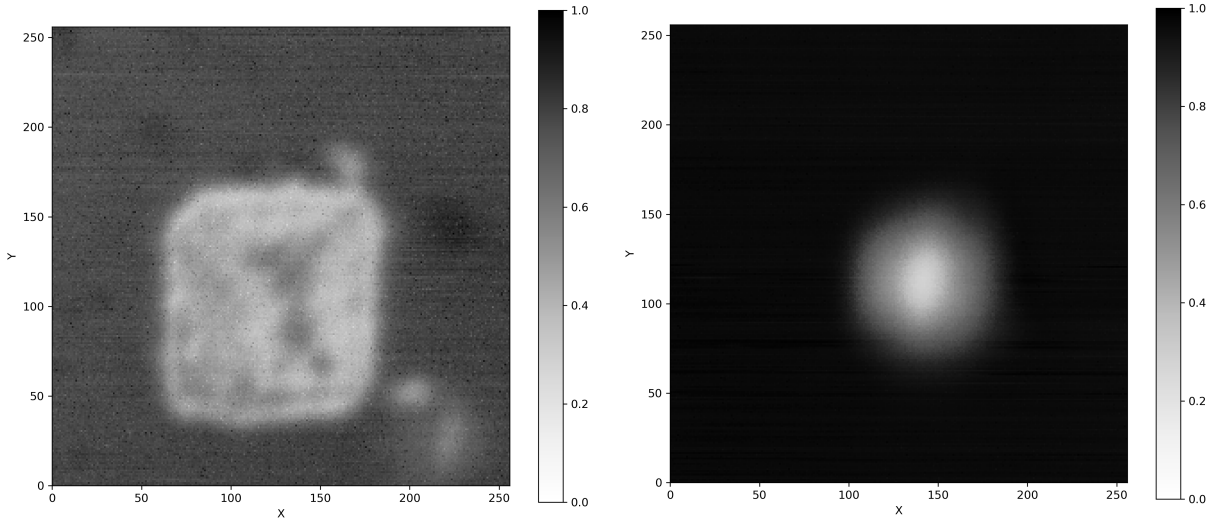

Figure 3.12: The 10x10µm chessboard is scanned with a very small stepsize with the 50x objective (left) and the 10x objective (right).

image of the 50x objective the structure can be still recognized as a square but the image taken with the 10x objective shows only a bright dot.
In this way, the resolution should be greater than 1μm and smaller than 10μm for both objectives. To precise it even more, the second way is used by measuring the burned lines of GST (see Figure 3.13).

For the measurements the smallest line are used, since the power was high enough that not only the areas directly in the focus point are burned but also some parts around. The smallest lines are created with less power. For the 50x objective the measurement gave a

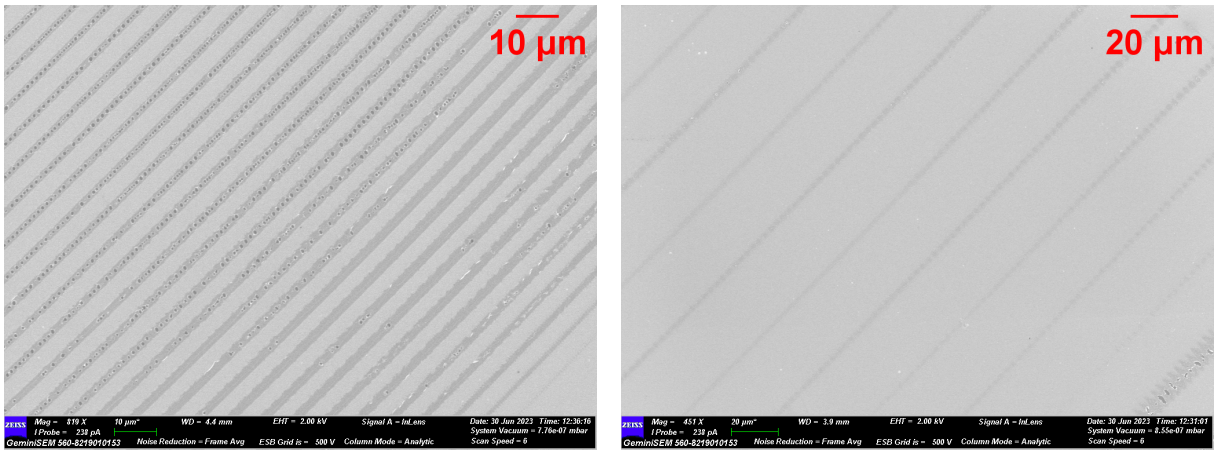

Figure 3.13: Lines are burned into the GST chip with the 50x objective (left) and the 10x objective (right). Afterwards the size was measured with a scanning-electron-microscope.

resolution of $(0.8 \pm 0.1)\mu$m and for the 10x objective $(1.6 \pm 0.2)\mu$m.
From this measurement it can be concluded that the optical setup in the Stage-static setup also has an influence on the image making process. For further investigations another calibration chip could be used with a chessboard size between 10 and 1μm.
For the Laser-static setup again a GST chip was burned with lines and as expected similar values are measured with a scanning-electron-microscope.
Mitutoyo states that there 50x objective should have a resolution of 0.42μm [34] and Edmund Optics states that the 10x objective should have a resolution of 1.0μm [35]. Since the resolution is wavelength dependent the values given are not correct for the whole wavelength range of the objectives. With the help of the Rayleigh-criteria an equation can be derived, calculating the possible resolution for each wavelength [48]:

$$R = \frac{0.61\lambda}{NA} \tag{3.5}$$

λ is the used wavelength and NA is the numerical aperture of the used objective. For the 50x objectives this gives a value of $R_{50x} = 0.7\mu$m and for the 10x objective $R_{10x} = 1.6\mu$m. As expected, these values are bigger than the ones given in the data sheets.
For the 10x objective the result of the measurement matches the the theoretical data, while for the 50x objective there is a small deviation. This difference can still be explained with a small distribution of the heat around the focus point, so that more than the hit part is burned.

In both of the setups it is difficult to position the chip at exactly the working distance of the used objective. Therefore, it is possible that the spot size hitting the chip is not the smallest possible, because the chip was either further or closer to the objective than

the working distance. Additionally, the holders for the chips are not completely even so that if the chip is moved the distance must always be corrected. The length scale of the unevenness was big enough to be recognized, while possibly also the chips are not completely even, but here the length scale would be so small, that it was not recognized with these setups.

3.4.4 Movement speed

One of the main reasons to use a Stage-static setup instead of a Laser-static setup is that a higher movement speed and therefore also a higher scanning speed can be achieved, due to a smaller mass that must be moved. Another reason could be that if the chip is connected with some wires or similar and then the movement of the chip would stress the connections and could lead to any damage.
Not only for scanning a higher speed can be interesting but also for switching the PCM cells. By considering a chip with a matrix pattern as mentioned in the introduction and connected waveguides, the limiting processing speed is mainly given by the time needed to switch all the PCM cells. The optimal movement speed would be so fast that pulses with the repetition rate $r_0 = (80 \pm 1)$MHz of the Mai-Tai laser do not overlap. Like this every laser pulse switches only one spot of the PCM cell.
The previous chapter about the resolution showed that the spot size is $s_{50} = (0.8 \pm 0.1)\mu$m for the 50x objective and $s_{10} = (1.6 \pm 0.2)\mu$m for the 50x objective. This means that the movement speed of the setups needs to be faster than:

$$s_{50} \cdot r_0 = (64 \pm 8) \cdot 10^6 \frac{\mu\text{m}}{\text{s}} \tag{3.6}$$

$$s_{10} \cdot r_0 = (128 \pm 16) \cdot 10^6 \frac{\mu\text{m}}{\text{s}} \tag{3.7}$$

If the speed is lower, the pulses will overlap. In the thesis of Björn Luig [26], he used the 50x objective and measured that the maximum speed of the Galvo is $(2100 \pm 210)\frac{\mu\text{m}}{\text{s}}$. Therefore the Galvo, is not fast enough even though he used the pulse-picker and reduced the repetition rate to $r_0 = (8 \pm 1)$MHz. By comparing different speeds below the threshold no difference of the switched surface was seen, that means the interesting speed is above the threshold.
Lin Jin also used in her Master thesis a Galvo system for switching GST, but this time with a 10x objective. The used speed was in that case $(120000)\frac{\mu\text{m}}{\text{s}}$ [49]. Even if the optical setups differ due to the telecentric lens system, the movement speed should be in the same order of magnitude with respect to the used objective. So no further investigations were done whether the speed has an influence on the switching or burning process or not, especially because without the pulse-picker it was not possible to reduce the repetition

rate.

In the software of the Laser-static setup, the movement speed of the stage can be varied, but there were no boundaries given. Even in the data sheet no maximum or minimum velocity was mentioned. That means, in theory it would be possible if the movement speed can go high enough to examine the influence of the movement speed on the switching process.

While measuring the burned lines for the resolution with the scanning-electron-microscope, some interesting structures were found and is shown in Figure 3.14.

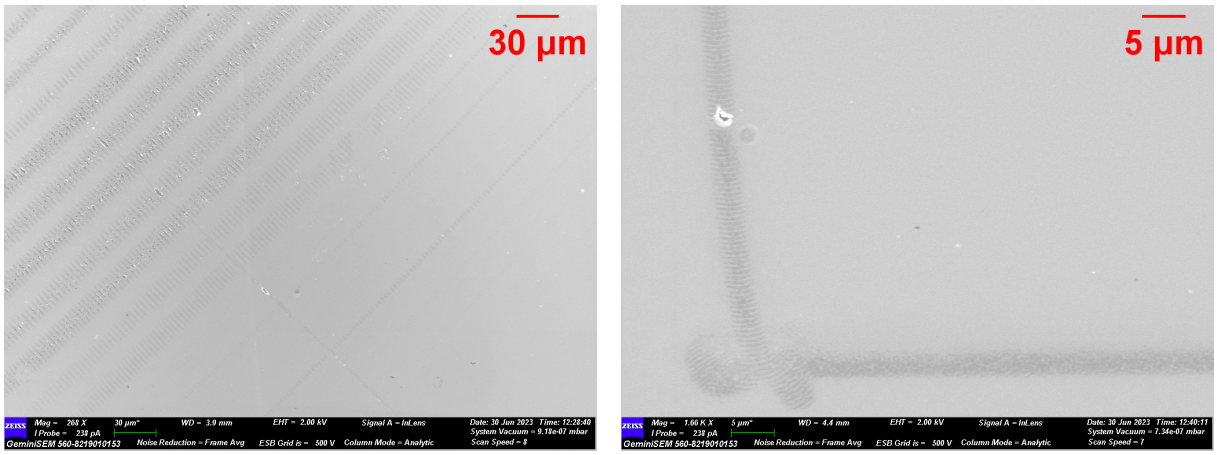

Figure 3.14: On the left the side, a closer look at the burned lines done with the 10x objective and the Stage-static setup is shown and on right side the lines are done with the Laser-static setup (with $20000\frac{\mu m}{s}$).

Interestingly, in the images the lines a clearly striped, even though it was said before, that the velocities of the Stage-static setup in general and also the one of the Laser-static setup are not high enough to make the focus points overlap. Additionally, the visible lines are not dotted as one would expect if the laser is hitting the GST not continuously but only partially. They lines have a more striped look. One possible explanation is that the motors moving the mirrors of the Galvo and also the motors of the stage are working as step motors, that they are always moving step wise in the chosen direction. This explanation could only work for the fact that a discontinuous structure can be seen but it does not explain why the lines are striped and not dotted. This sort of lines is not visible in the structures made with the Stage-static setup and the 50x objective, which could fit to the explanation regarding the step motors, since there the step size projected on the chip is probably so small that the stripes overlap and form a continuous line.

3.4.5 Conclusion

The goal was to find the more suitable setup for switching GST on a chip. Therefore four criteria were compared. The possible movement area was the first criterion. Here the Stage-static setup is much better, since with the usage of the 50x objective the possible movement in x and y direction was nearly three times bigger and with the 10x objective around ten times bigger than with the usage of the Laser-static setup. For the second criterion, the power fluctuations within the movement area, the Laser-static setup is better than the Stage-static, especially when using the 50x objective. This is because there the fluctuation where quite high and for the 10x objective there were still some fluctuation on the outer area. Nevertheless, if only the inner part is used, the fluctuation are minimal. Regarding the resolution the results are - as expected - the same for the two setups, since this is given by the used objective. For the last criterion, the movement speed, it was found that the Stage-static setup is not fast enough to prevent the focus points of overlapping, even if one would use the pulse-picker. For the Laser-static setup, some further measurements or information would be needed to finally decide whether it is fast enough or not, since in the software there are no boundaries given for the maximum speed.
To conclude, the Stage-static setup with the 50x objective is not suitable for switching GST, because the power fluctuations are too high, since the correct power is really important as it will be shown in the next chapter. The Laser-static setup and also the Stage-static setup with the 10x objective are both suitable but the Stage-static has the bigger movement area while the Laser-static could have the higher movement speed.
For further investigation, another criterion for the Laser-static setup could be examined: The accuracy of the movement. If for example a fiber array is placed above the chip and aligned with some grating couplers on the chip it is very important that the chip is at the exact same position after a movement for switching a PCM cell. Since the chip in the Stage-static setup is not moved this could be a huge advantage.
Additionally, it was possible to take images with the Stage-static setup with a resolution close to the ones given by the objective. Nevertheless, a disadvantage of a scanning microscope is the long time for taking images, since every pixel is done one after the other. That means, when the pixel number is increased, also the time of the image-taking process increases.

4 Switching PCM

In the previous chapter, a chip covered with GST was already used to characterize the different setups. For all measurements the GST was burned instead of switched. From the theory it is known that for switching GST to the amorphous state, a specific amount of energy is needed to heat it up high enough, but not too high to burn it. So the first step is to study the adjustable power reduction by the attenuator. In the ideal case, it would not always be necessary to measure the power at the chip, instead it can be calculated from the angle of the attenuator.

4.1 Power reduction through the attenuator

To measure the reduction of the power, the waveplate of the attenuator is rotated in all possible angles and the power is measured every time. These measurements can be seen in Figure 4.1. The uncertainties of the power ± 0.0012 and angle $\pm 0.00001°$ measurements are so small, that they cannot be seen in plots. Only the relative power is plotted, because

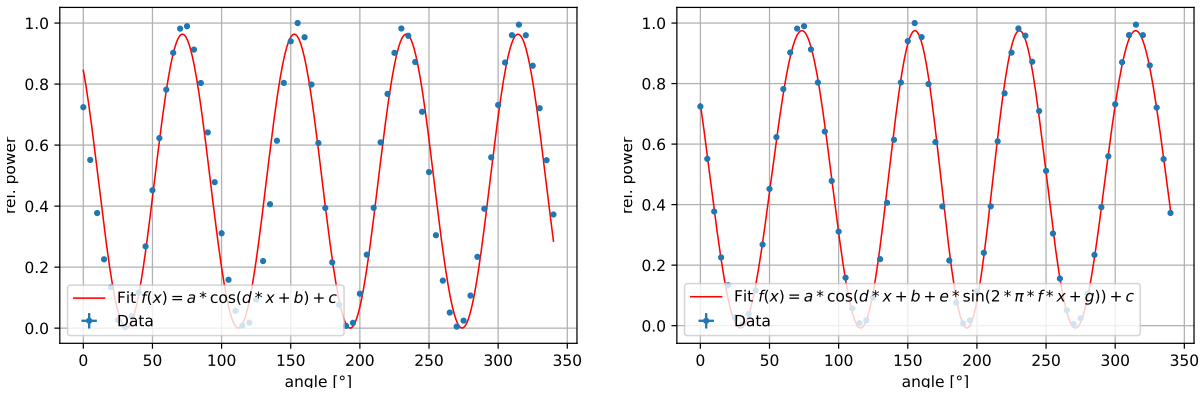

Figure 4.1: On both sides, the same measured data is plotted. On the left side only Malus's law is fitted, while on the right side an additional frequency modulation is used.

the absolute value of the power can highly differ depending on the position of the power meter, for example the power is much higher if it is placed directly behind the attenuator than if it is placed underneath the objective in the Stage-static setup. All these additional reductions could be investigated with further measurements.

In the theory it was predicted that the power should follow Malus's law, so in the left image of Figure 4.1 this law was used as the fit function and the result for the parameters is:

$$f(x) = (0.482 \pm 0.013) \cdot \cos\left((0.0777 \pm 0.0003) \cdot x + (69.83 \pm 0.05)\right) + (0.482 \pm 0.009) \tag{4.1}$$

However, for example in the range of 100° to 150° a clear systematic deviation can be seen, which indicates that the used function is not correct. By leaving the angle of the attenuator at one position and observing the power measurement, a periodic fluctuation was recognizable. This realization lead to the new function: a frequency modulated Malus's law.

$$P(2\alpha) = \frac{P_0}{2}\cos(4\alpha + \sin(2\pi f \alpha)) + \frac{P_0}{2} \tag{4.2}$$

It is important to mention that the measurement of the power was done in such a way that the angle could also represent time, since all the measurements were done directly one after the other and it took around 5s for each measurement. Therefore the new approach including the frequency modulation can be used. In the right image of Figure 4.1 the data with the fit function can be seen and the result for the parameters is:

$$\begin{aligned} f(x) = (0.491 \pm 0.003) \cdot \cos((0.07724 \pm 0.00019) \cdot x + (69.89 \pm 0.03) + (0.297 \pm 0.013) \\ \cdot \sin(2\pi(0.00366 \pm 0.00013) \cdot x + (-4.26 \pm 0.16))) + (0.4835 \pm 0.0024) \end{aligned} \tag{4.3}$$

This time no systematic deviation is visible anymore, therefore is looks like the used fit function is describing the measurement more properly. However the results of the fit parameter are only a first approximation because the time for each measurement was not noted and therefore and it was not the goal in the beginning to also include this. Since the measurement of the angle of the attenuator is very precise, the only conclusion is that the polarization of the Mai-Tai laser is changing all the time.

With this information, a next step could be to set the attenuator to a angle and just measure the power behind it. In this way, the time-dependent polarization change could be measured. Additionally, the influence of turning the laser on and off would have to be considered, since the polarization could change here abruptly.

To find a function calculating the power of the laser beam by just inserting the angle of the power meter is complicated, especially to prove that there are no further effects which have not yet been named. Therefore, in this thesis the power was always directly measured underneath the objective in the moment of use so that the time dependent change can be neglected.

4.2 Switching of GST

The main goal of this thesis is to use the previously described setups to reversibly switch GST from the crystalline state to the amorphous state, but only in this one direction. For the other direction, from amorphous to crystalline, the duration of the laser pulse should be changeable. Therefore, for this process a hotplate is used.
To change the chip to crystalline, it is first cleaned with acetone in a sonic bath and afterwards the acetone is removed with isopropyl alcohol. Then the chip is placed on a hotplate at 250°C for 15 minutes and afterwards cooled down to room temperature. In this way all the GST should be in the crystalline state after this procedure.
This first chip used is covered with a 10nm layer of GST. It was placed underneath the objective in the Laser-static setup and by adjusting the height, the laser was focused on the top of the chip. In the first try, the average power was set to around 60mW and was gradually reduced from there. This initial amount of power was used because it was known from previous tests that the GST gets burned and the structure can be found with a microscope. This first attempt can be seen in Figure 4.2.

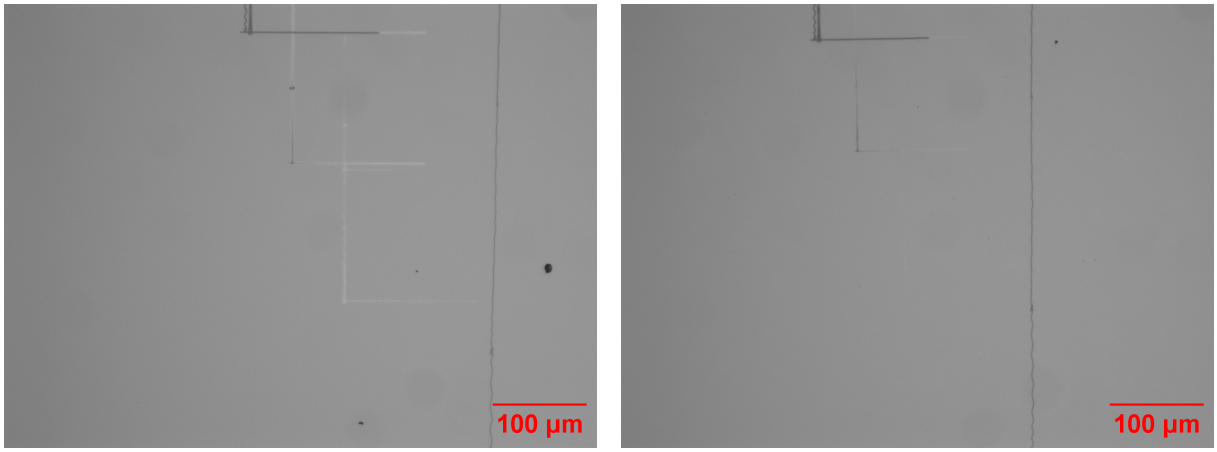

Figure 4.2: Four different powers were used to create amorphous structures on the chip. The step in the left image is the first one with around 60mW, then, going to the right, the next one with 35mW, then 17mW and the last structure with 7mW, which is not visible anymore. The left image was done directly after the usage of the laser and the right one after recrystallizing.

The unequal step size of the power is due to the fact that the angle of the attenuator was changed in equal steps and then the power was measured, but since the angle is not representative only the power value is noted. In the left image, only three step-like structures can be seen, with the second and third one showing mainly white color, not dark grey as for the first one. By comparing it to the right image, it can be seen that the

white color indicates amorphous structures, since the lines on this side disappeared which is caused by a change back to the crystalline state. The conclusion of this measurement is that switching GST is possible with an average power of 17 to 35mW. Worth noticing is the corner of 35mW the step done is also burned, so it looks like this power is close to the maximum for reversible switching.
In the next measurement, the previously found power range was examined more closely. Again, some lines were created with an average power high enough to burn it, so that it is possible to find the structure even after recrystallizing. This time, more and smaller angle settings of the attenuator are used, so that 20 lines could be visible within a burned square. An image of the result can be seen in Figure 4.3.

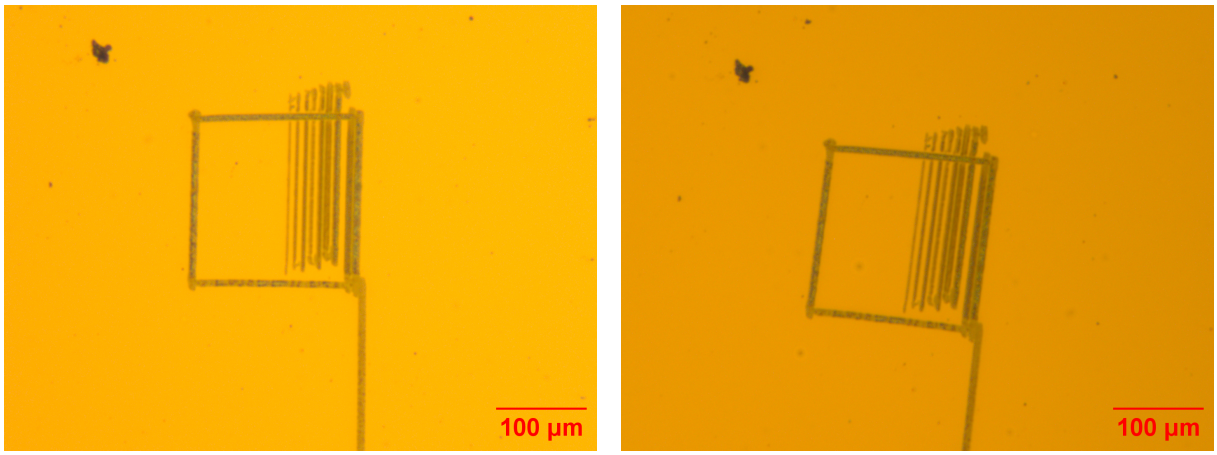

Figure 4.3: Within the square of burned GST, 20 different power settings were used to find the right amount of power to switch the GST to the amorphous state. On the left side, the image was taken again directly after it was hit with the laser and on the right side the image was taken after the hotplate. This time another camera was used which can take color pictures.

The first observation is that only eight out of 20 lines are visible, so one could expect that there are some burned lines, amorphous lines and also some parts where the GST stayed in the crystalline state. Interestingly only burned lines are visible and nothing more, That means there were no amorphous lines at all. The last visible line was done with an average power of 42mW and the next one, which already is not visible anymore, with 35mW. This result shows already a contradiction to the one of the first attempt where at the power of 35mW the GST was switched to the amorphous state and this time no lines were created with 35mW.
Additionally, this time it was supervised whether the laser was pulsing or not. The result shows that exactly at the transition point between no lines and burned lines the pulsing changed. This means that the burned lines were done with a continuous laser beam and

the lines which are not visible are done with a pulsed laser beam. Since this makes a big difference in the heating process of the chip, it is important to consider it in the evaluation of the used average power.
With this knowledge, multiple further attempts were carried out with the same procedure as before to find the right settings to switch the GST. The first results were not reproducible. However, other unexpected observation were made.
One observation is that the lines which are expected to be burned have some interesting shape after the recrystallization (see Figure 4.4). The lines are made of spots and are not

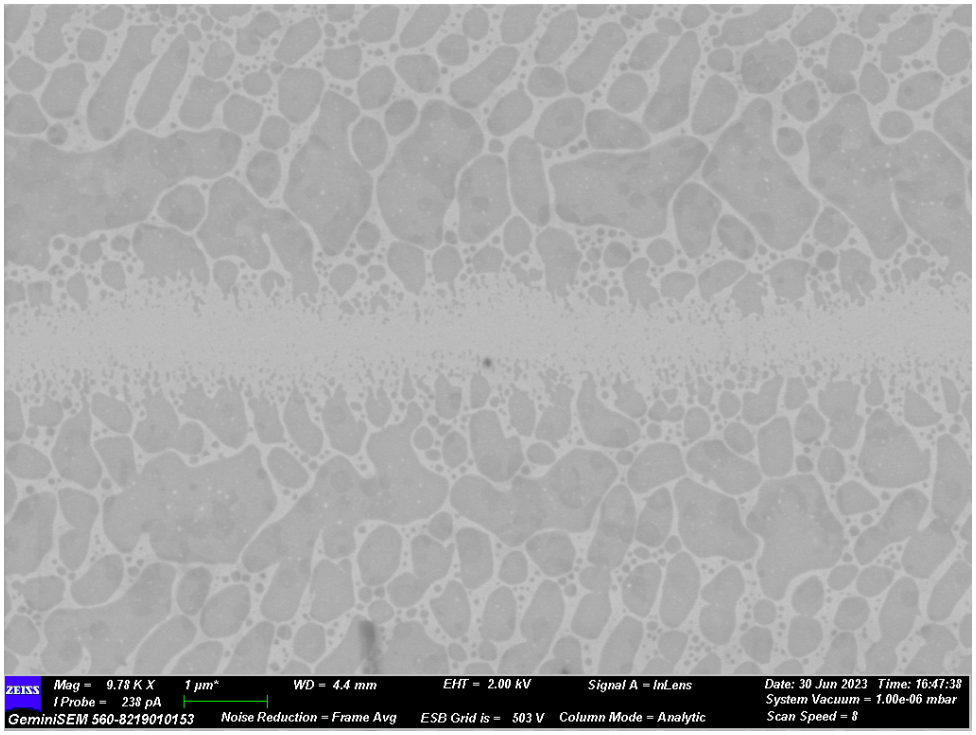

Figure 4.4: A closeup of two burned lines is shown. These lines are separated by a small line of remained crystalline GST in the middle. The image was taken with a scanning electron microscope.

homogeneous. This type of shape reminds of a nucleation process because at the edge of the lines the spots are smaller and in the middle of the lines is looks like multiple spots connected themselves to form bigger ones. This is unexpected since the GST started in a crystalline state and the goal was to create an unordered amorphous state.
Another observation is the small white grains within the large dark grey spots. As they have the same color as the other crystalline parts it is possible that these grains form some kind of polycrystalline structure, which would mean that the GST was unable to create one whole crystal again.
At this point of measurement the chip broke accidentally because of a too strong adhesive for the electron microscope, that's why it was possible to carry out multiple test to further

understand the recrystallization process with the same original chip. One piece was then heated for one hour at 250°C and three pieces were heated to 250°C, 260°C and 270°C for just 15 minutes. Afterwards the chips were scanned again with an electron microscope, but no changes in the structure were visible.

A third observation is that the power needed for burning the GST always increased after each recrystallization. Especially for the pieces heated up to more than 250°C and the one heated up for an hour, the power needed was then far higher than 100mW.
A possible explanation could be that the GST is oxidized, since it is directly exposed to the air. This oxidation causes a change in the structure of the GST, as the Sb and the Ge are forming oxides instead of connections with the Te. If the crystallization is done at higher temperatures, a Ge-rich phase can be found in the top 10nm of the GST structure [50]. Since the layer of the GST used here is only 10nm thick, the whole lattice structure could be changed. Additionally, the crystallization temperature changes significantly dependent on the oxygen concentration in the GST [51][52]. Therefore, also the temperature required to switch to the amorphous state could change.
An idea to reduce the influence of the oxidation process is to cover the GST with another material. Following this idea, a new chip was used on which a 5nm Aluminum oxide layer is put on top of the 10nm GST layer. With this newly layered chip the same tests are carried out as with the one before to create some reference structure through burning the GST and then reducing the power to find the right amount of power to switch the GST to an amorphous state. In Figure 4.5 one of these test patterns can be seen.

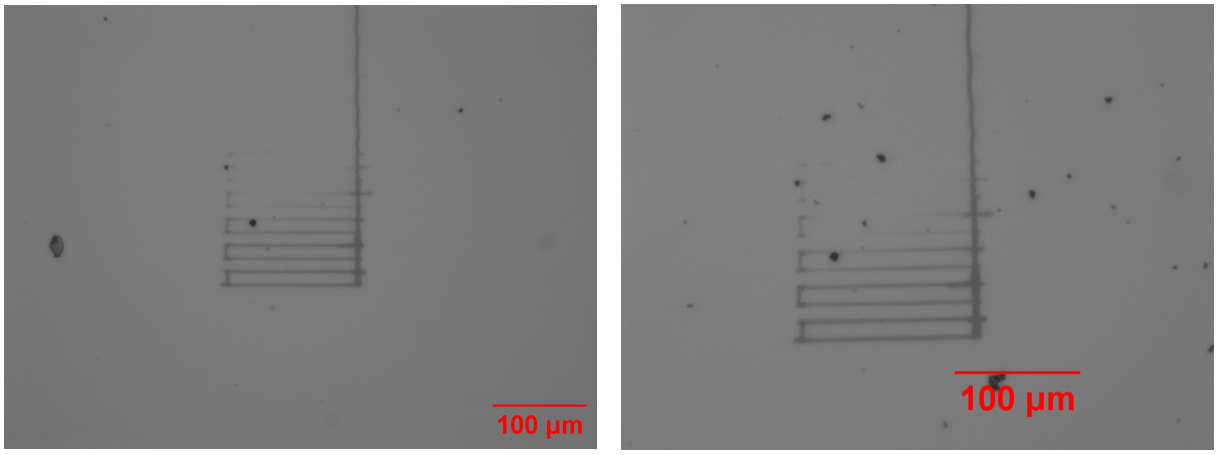

Figure 4.5: On the left side, eleven lines are visible, created by five different power settings, while on the right the same lines are shown after the recrystallization process.

As before, the same problem with the chip occurred; either the GST is burned or nothing

happened, so that no intermediate step could be found. This time, the transition was at around 34mW. Interestingly, in one of the first test structures, it looked like an amorphous structure was created, even though it was not intended (see Figure 4.6). Since this happened while testing for the right amount of power to burn the chip, the power was not measured. However, the line was still visible even though the chip was heated up at 250°C for 15 min. This result is very unexpected, because in the measurements of the previous chip the white color was indicative of an amorphous structure, which then disappeared during the similar heating process.

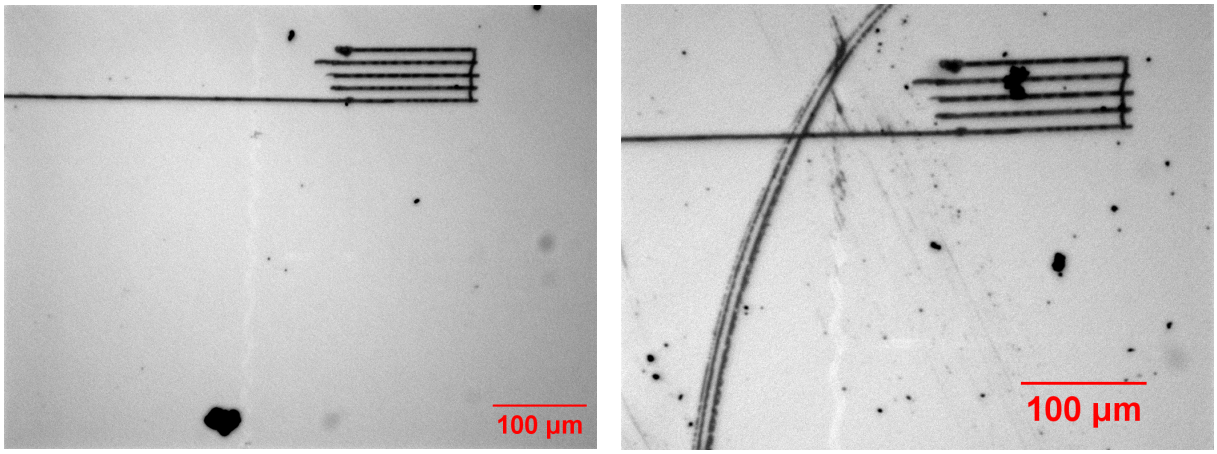

Figure 4.6: The main focus of the images lies on the white line. The image on the left side was taken after the chip was hit with the laser. The image on the right side was taken after the chip was heated with the hotplate but the white line is still visible.

These tests with the second chip show that, even though oxidation could still be a problem, it is not the main one, since the chip was only heated at 200°C for 10 minutes in the first heating process and is covered with Aluminum oxide. This could cause some diffusion, but as it was still possible to switch the GST accidentally another explanation is needed.
For Niklas Hesse and Björn Luig it was possible to switch the GST with a very similar setup. One crucial difference between their setup and the one used here is the pulse-picker, because they used a repetition rate of (8.0 ± 0.1)MHz for the laser pulses instead of the (80 ± 1)MHz [25][26]. Therefore, the time between the pulses is 125ns for the 8MHz and 12.5ns for the 80MHz. This small time of the repetition rate without the pulse-picker could already be the problem, because the vitrification process is equally fast. Additionally, this process could also be dependent on the pulse duration, since for example in the case of using GeSb thin films, the amorphization takes around 10 to 15ns if pulses in the femtosecond regime are used. By increasing the pulse duration the transformation time

is reduced [53]. If the amorphization time for the GST has the same order of magnitude and the incoming energy is greater than the dissipation of energy through the air, the consequence would be that the GST is not cooled down completely between two laser pulses. This would mean that the energy or heat is added up and the GST is burned. In addition to that, at the equilibrium, if the incoming energy amount is equal to the removed amount through the cooling process between two laser pulses, the heat is not sufficient that the GST reaches the melting temperature. In conclusion it can be said, that either the repetition rate is too high or the cooling process too slow. Since in theory it is possible to change the repetition rate with the pulse-picker, its influence on switching GST could be studied by varying its rate.

5 Limits of the Out-of-plane setup

During the use of the two out-of-plane setups, various limitations and shortcomings were found. The first one is the limited range of the setups, either given by the movement range of the stage or given mainly by the used objective. Therefore, the dimensions for example of a matrix is then give by this movement area. Also the resolution and thereby the size of a PCM cell as well are given by the used objective, especially if a PCM cell should only be hit partially.
Another shortcoming is that either an additional setup is needed for connecting a fiber array with the grating couplers or the used objectives need to have a long working distance though this often goes together with a smaller magnification.
A third point of limitation of the setups is the complexity of their construction. Especially placing the chip in the working distance can be challenging as every component is imperfect; the stage for example can be uneven. Another point is that the space needed for the Stage-static setup is very large and nevertheless only a small part of the chip can be controlled.
The limitation of the speed is given by the used Galvo or stage, since in this case they cannot move fast enough to prevent the focus points of overlapping.
Another main problem observed in the previous part is that the out-of-plane setups are very dependent on the used chip, so that the use of cover materials and their composition have big impact on the results. Therefore the used power always has to be adapted. Regarding this feature, an in-plane setup has it benefits, since here the PCM can be directly connected via a waveguide or an electrical connection and only be covered with any type of material afterwards.

6 Conclusion and Outlook

Artificial intelligence plays an increasingly important role in daily life, like in the use of image and voice recognition or in the field of autonomous driving. In general the demand for artificial neural networks is steadily increasing with the consequence that conventional computers are reaching their limits in processing speed, physical size and energy efficiency. So one way to deal with this challenge is the use of photonic integrated circuits, especially the photonic matrix tensor cores. For this, phase-change material cells are used as the weights and the goal is to switch them with an out-of-plane setup.
The main goal of this thesis was to compare two possible setups for this switching process: the Stage-static and the Laser-static setup. Both of them were designed partly with templates from other theses, then constructed and in the end tested and evaluated.
It was found that the Stage-static setup with the 10x objective has the biggest movement area with $(1550 \pm 40)\mu$m in x direction and $(1560 \pm 40)\mu$m y direction but would loose some of this area during its use in the switching process due to high power fluctuations in the outer areas. Regarding this feature, the Laser-static setup is the better one, since only the stage is moving and the light path stays static. The fact that only around 25% of the movement area can be used during the usage of a 50x objective in the Stage-static setup shows its enormous problems with the power fluctuations.
The resolution in the switching process was expected to mainly dependent on the used objective. Here a spot size of $(1.6\pm0.2)\mu$m for the 10x objective while for the 50x objective $(0.8 \pm 0.1)\mu$m was obtained. In the next step, it would be interesting to compare these sizes with the size of a PCM cell to see whether it is also possible to switch a cell partially. One benefit of the 10x objective is the bigger working distance than the one of the 50x objective. Because of that, it is possible to align a fiber array on top of grating couplers on a chip without bending the fibers strongly or even damaging them. Like this it would be possible to build a setup directly including the possibility to measure the transmission through waveguides with PCM cells on top.
Moreover, it was possible to use the Stage-static setup as a confocal microscope with a resolution in the order of a few micrometers. To get a more precise value for the scanning resolution, another calibration chip would be needed with more structures in this size.
In the last part of the thesis the goal was then to actually use the compared setups to switch GST, but unfortunately it did not work reproducibly. The problem was that

contrary to the assumptions, no amorphous structure was created; with changing power the GST only burned or did not change at all. To find an explanation for this, two different chips were used in a following experiment and studied with a scanning electron microscope: one with only GST one with a layer of Aluminium oxide on top of the GST. During that experiment, some interesting patterns were found with the before mentioned microscope like for example the discontinuous burned lines made out of spots with some grains inside (see Figure 4.4). Another unexpected result are the striped lines made by the Stage-static and the Laser-static setup (see Figure 3.14). For the striped line the explanation is that the motors of the Galvo and the stage are working stepwise, but still then a dotted line would be expected, so there are also some other unknown effects.
Regarding the switching problem, two different hypotheses were set up. Firstly that GST oxidizes and therefore changes its lattice structure and its properties and secondly, that the repetition rate of the laser is too high, so that the GST cannot cool down between two pulses, or is not heated up enough to reach the melting temperature.
The oxidation could be observed with an transmission electron microscope, but the effect can be reduced by using a protection layer. The influence of a too high repetition rate can be studied with the help of the pulse picker. In general another approach to find out in which state the GST is, a backloop structure could be used. In this way the switching process could be described more quantitatively instead the qualitative observation with the microscope. These backloop structures consist of one waveguide which is divided into two. On one of them a GST cell is placed. The transmission is measured through both arms and then compared to study the influence of the GST. If the phase is then changed, the transmission should also change. This measurement can then be done before exposing the GST to the laser, afterwards and again after the the chip in heated up with the hotplate. It is then expected that the transmission is the same before the expose and after the hotplate, so in this case the GST would be in a crystalline state before and afterwards.
In general, it can be said for both setups, that is was difficult to position the chip in the working distance of the objectives, this could still be improved to make the results more reliable. This could be done for example with an electrical moved stage, instead of a manual one. Additionally, the alignment of the telecentric lens system and the cylindrical lenses of the Stage-static setup can still be improved, since this is the crucial point of quality of the setup, especially regarding the power fluctuations. For this an additional laser could be used, placed at the position of the chip. The goal is then to align the lenses in such a way that the laser are focused at the same position.
Also the Laser-setup can be improved in order to have less back reflections and a bigger power range with a pulsed laser beam transmitted through the optical fiber. Here already the usage of the pulse picker would help.

7 Appendix

7.1 Acknowledgements

At this point I want to thank my supervisor Shabnam Taheriniya, who was always there when I had questions or if parts for the different setups were needed. Especially the images done by her with the electron microscope helped a lot and gave a new possibility to study the behavior of the GST. Additionally, I also want to thank Prof. Dr. Wolfram Pernice to provide me the opportunity to write my bachelor thesis in his group. Also many thanks to all group members who were always very friendly and helpful.

7.2 Declaration

Ich versichere, dass ich diese Bachelorarbeit "Stage-static and Laser-static Out-of-Plane Setups for Switching Phase-Change Materials" selbstständig verfasst und keine anderen als die angegebenen Quellen und Hilfsmittel benutzt habe.

Heidelberg, den 29.07.2023 Julius Delme

7.3 Code

The python code for the scanning microscope:

```
import tkinter as tk
import numpy as np
import matplotlib.pyplot as plt
from matplotlib.backends.backend_tkagg import (FigureCanvasTkAgg)
import nidaqmx

root = tk.Tk()
root.title('Powermeter Measurement')
left_frame = tk.Frame(root)
right_frame = tk.Frame(root)

fig, ax = plt.subplots(ncols = 1, figsize=(10,8))

im_2 = ax.imshow(data, cmap='Greys', interpolation = None, origin='lower
    ', norm=None, vmin=0.0, vmax=1.0)
cbar = ax.figure.colorbar(im_2, ax=ax)
ax.set_xlabel("X")
ax.set_ylabel("Y")

canvas = FigureCanvasTkAgg(fig, master=right_frame)
canvas.draw()

plotting_active = False
data = np.zeros((1,1))
zero = 0
y = np.array([])
duration = np.array([])

def zeroing():
    global zero
    with nidaqmx.Task() as task:
        task.ai_channels.add_ai_voltage_chan("PXI1Slot2/"+selected_input
    .get())
        measurement_values = task.read(number_of_samples_per_channel=int
    (average_zero_spinbox.get()))
        zeros = np.append(zero, np.asarray(measurement_values, dtype=
    float))
    zero = np.mean(zeros)

def get_value():
    global zero
    values = np.array([])
```

```
39      with nidaqmx.Task() as task:
40          task.ai_channels.add_ai_voltage_chan("PXI1Slot2/"+selected_input
    .get())
41          measurement_values = task.read(number_of_samples_per_channel=int
    (average_spinbox.get()))
42          values = np.append(values, np.asarray(measurement_values, dtype=
    float))
43      return np.mean(values) - zero
44
45  def scanning():
46      global plotting_active, master_active, data, master_flat_field,
    master_flat_field_norm, counter_x, counter_y, volts_x, volts_y,
    duration
47
48      with nidaqmx.Task() as task:
49          task.ao_channels.add_ao_voltage_chan("PXI1Slot2/ao0", min_val
    =-10, max_val=10)
50          task.write(volts_x[counter_x])
51      with nidaqmx.Task() as task:
52          task.ao_channels.add_ao_voltage_chan("PXI1Slot2/ao1", min_val
    =-10, max_val=10)
53          task.write(volts_y[counter_y])
54      data[counter_y][counter_x] = get_value()
55      counter_x += 1
56      if counter_x == int(pixel_num_spinbox.get()):
57          print(counter_y)
58          counter_x = 0
59          counter_y +=1
60
61      if counter_y == int(pixel_num_spinbox.get()):
62          master_active = False
63          plotting_active = False
64          data_max = np.max(data)
65          data = data/ data_max
66          im_2 = ax.imshow(data, cmap='Greys', interpolation = None,
    origin='lower', norm=None, vmin=0.0, vmax=1.0, extent=[0,int(
    pixel_num_spinbox.get()),0,int(pixel_num_spinbox.get())])
67          canvas.draw()
68          plt.show()
69          ax.figure.savefig('10x Objective.png', dpi=300)
70
71      if plotting_active:
72          root.after_idle(scanning)
73
74  def scan_plot():
75      global data, counter_x, counter_y, volts_x, volts_y
```

```
76      data = np.zeros((int(pixel_num_spinbox.get()),int(pixel_num_spinbox.
        get())))
77      counter_x = 0
78      counter_y = 0
79      volts_x = np.linspace(float(volts_minx.get()),float(volts_maxx.get()
        ), int(pixel_num_spinbox.get()))
80      volts_y = np.linspace(float(volts_miny.get()),float(volts_maxy.get()
        ), int(pixel_num_spinbox.get()))
81      scanning()
82
83
84  def start_plot():
85      global plotting_active
86      if not plotting_active:
87          plotting_active = True
88          scan_plot()
89
90  def stop_plot():
91      global plotting_active
92      plotting_active = False
93
94  inputs = ['ai0', 'ai1', 'ai2', 'ai3', 'ai4', 'ai7']
95  selected_input = tk.StringVar()
96  selected_input.set(inputs[5])
97
98  num_averages = [1, 5, 10, 50, 100]
99
100 num_zero_averages = [1, 5, 10, 50, 100]
101
102 num_pixel = [8, 16, 32, 64, 128, 256, 512, 1024]
103
104 input_label = tk.Label(left_frame , text='Select Input')
105 input_menu = tk.OptionMenu(left_frame , selected_input, *inputs)
106
107 average_label = tk.Label(left_frame , text='Number of Averages:')
108 average_spinbox = tk.Spinbox(left_frame , values=num_averages)
109
110 average_zero_label = tk.Label(left_frame , text='Number of Averages for
        Zeroing:')
111 average_zero_spinbox = tk.Spinbox(left_frame , values=num_zero_averages)
112
113 zeroing_button = tk.Button(left_frame , text='Zeroing', command=zeroing)
114
115 volts_minx_label = tk.Label(left_frame , text='x_min')
116 volts_minx = tk.Entry(left_frame)
117 volts_minx.insert(0,'0')
```

```
118
119 volts_maxx_label = tk.Label(left_frame , text='x_max')
120 volts_maxx = tk.Entry(left_frame)
121 volts_maxx.insert(0,'0')
122
123 volts_miny_label = tk.Label(left_frame , text='y_min')
124 volts_miny = tk.Entry(left_frame)
125 volts_miny.insert(0,'0')
126
127 volts_maxy_label = tk.Label(left_frame , text='y_max')
128 volts_maxy = tk.Entry(left_frame)
129 volts_maxy.insert(0,'0')
130
131 pixel_num_label = tk.Label(left_frame , text='DPI:')
132 pixel_num_spinbox = tk.Spinbox(left_frame , values=num_pixel)
133
134 plotting_button = tk.Button(left_frame , text='Start Measurement',
    command=start_plot)
135
136 stop_button = tk.Button(left_frame , text='Stop Measurement', command=
    stop_plot)
137
138 input_label.pack()
139 input_menu.pack()
140
141 average_label.pack()
142 average_spinbox.pack()
143
144 average_zero_label.pack()
145 average_zero_spinbox.pack()
146
147 zeroing_button.pack()
148
149 volts_minx_label.pack()
150 volts_minx.pack()
151 volts_maxx_label.pack()
152 volts_maxx.pack()
153 volts_miny_label.pack()
154 volts_miny.pack()
155 volts_maxy_label.pack()
156 volts_maxy.pack()
157
158 pixel_num_label.pack()
159 pixel_num_spinbox.pack()
160
161 plotting_button.pack()
```

```
162 stop_button.pack()
163
164 canvas.get_tk_widget().pack()
165
166 left_frame.pack(side = 'left')
167 right_frame.pack(side = 'right')
168
169
170 root.mainloop()
```

The python code for the test patterns, done with the Stage-static setup:

```
import numpy as np
import nidaqmx
import time

with nidaqmx.Task() as task:
    task.ao_channels.add_ao_voltage_chan("PXI1Slot2/ao0", min_val=-10, max_val=10)
    task.ao_channels.add_ao_voltage_chan("PXI1Slot2/ao1", min_val=-10, max_val=10)

    x_min = -5
    x_max = 5

    y_min = -5
    y_max = 5

    num_lines = 20

    # increasing Power at every line
    y = np.linspace(y_min, y_max, num_lines)
    print(y)
    task.write([x_min,y[0]])
    input("Press any key to start")

    for j in range(num_lines):
        if j % 2:
            task.write([x_min,y[j]])
            time.sleep(0.000001)
            #print('finished line1')
            #input("Press any key to continue")
        else:
            task.write([x_max,y[j]])
            time.sleep(0.000001)
            #print('finished line2')
            #input("Press any key to continue")


    #task.write([-10,-10])


    # Line Pattern for movement area with short stopping at num_lines points in between

    '''
```

```
42
43      x = np.linspace(x_min, x_max, num_lines)
44      y = np.linspace(y_min, y_max, num_lines)
45
46      for j in range(num_lines):
47          for i in range(num_lines):
48              #task.write([x[j],y[i]])
49              print([x[j],y[i]])
50
51      #task.write(-10,-10)
52      '''
53
54      # Line Pattern with increasing distance for resolution
55
56      '''
57
58      x = np.logspace(np.log10(1), np.log10(np.abs(x_min)+np.abs(x_max) +
    1), num_lines) - np.abs(x_min) - 1
59      y = np.linspace(y_min, y_max, num_lines)
60
61      for j in range(num_lines):
62          for i in range(num_lines):
63              #task.write([x[j],y[i]])
64              print([x[j],y[i]])
65
66      #task.write(-10,-10)
67
68      '''
```

References

[1] Roberto Gozalo-Brizuela and Eduardo C. Garrido-Merchan. "ChatGPT is not all you need. A State of the Art Review of large Generative AI models". In: (2023). arXiv: 2301.04655 [cs.LG].

[2] Tambiama Madiega. "Artificial intelligence act". In: *EPRS — European Parliamentary Research Service* (2023). URL: https://www.europarl.europa.eu/news/en/headlines/society/20230601STO93804/eu-ai-act-first-regulation-on-artificial-intelligence.

[3] Raman Chandrasekar. "Elementary? Question answering, IBM's Watson, and the Jeopardy! challenge". In: *Resonance* 19 (2014), pp. 222–241. DOI: 10.1007/s12045-014-0029-7. URL: https://doi.org/10.1007/s12045-014-0029-7.

[4] David Silver et al. "Mastering the game of Go with deep neural networks and tree search". In: *Nature* 529 (2016), pp. 484–489. DOI: 10.1038/nature16961. URL: https://doi.org/10.1038/nature16961.

[5] Robert A. Nawrocki, Richard M. Voyles, and Sean E. Shaheen. "A Mini Review of Neuromorphic Architectures and Implementations". In: *IEEE Transactions on Electron Devices* 63.10 (2016), pp. 3819–3829. DOI: 10.1109/TED.2016.2598413.

[6] Gaurav Batra et al. "Artificial-intelligence hardware: New opportunities for semiconductor companies". In: (2019). URL: https://www.mckinsey.com/industries/semiconductors/our-insights/artificial-intelligence-hardware-new-opportunities-for-semiconductor-companies#/.

[7] M. Mitchell Waldrop. "The chips are down for Moore's law". In: *Nature* 530 (2016), pp. 144–147. DOI: 10.1038/530144a. URL: https://www.nature.com/news/the-chips-are-down-for-moore-s-law-1.19338.

[8] J. Feldmann et al. "Parallel convolutional processing using an integrated photonic tensor core". In: *Nature* 589 (2021), pp. 52–58. DOI: 10.1038/s41586-020-03070-1. URL: https://doi.org/10.1038/s41586-020-03070-1.

[9] Simone Raoux. "Phase Change Materials". In: *Annual Review of Materials Research* 39.1 (2009), pp. 25–48. DOI: 10.1146/annurev-matsci-082908-145405. URL: https://doi.org/10.1146/annurev-matsci-082908-145405.

[10] Frank Brückerhoff-Plückelmann et al. “Chalcogenide phase-change devices for neuromorphic photonic computing”. In: *Journal of Applied Physics* 129.15 (Apr. 2021), p. 151103. ISSN: 0021-8979. DOI: 10.1063/5.0042549. eprint: https://pubs.aip.org/aip/jap/article-pdf/doi/10.1063/5.0042549/15260222/151103_1_online.pdf. URL: https://doi.org/10.1063/5.0042549.

[11] Matthias Stegmaier et al. “Nonvolatile All-Optical 1 × 2 Switch for Chipscale Photonic Networks”. In: *Advanced Optical Materials* 5.1 (2017), p. 1600346. DOI: https://doi.org/10.1002/adom.201600346. eprint: https://onlinelibrary.wiley.com/doi/pdf/10.1002/adom.201600346. URL: https://onlinelibrary.wiley.com/doi/abs/10.1002/adom.201600346.

[12] Daiki Tanaka et al. “Ultra-small, self-holding, optical gate switch using Ge2Sb2Te5 with a multi-mode Si waveguide”. In: *Opt. Express* 20.9 (Apr. 2012), pp. 10283–10294. DOI: 10.1364/OE.20.010283. URL: https://opg.optica.org/oe/abstract.cfm?URI=oe-20-9-10283.

[13] Sajjad Abdollahramezani et al. “Tunable nanophotonics enabled by chalcogenide phase-change materials”. In: *Nanophotonics* 9.5 (May 2020), pp. 1189–1241. DOI: 10.1515/nanoph-2020-0039. URL: https://doi.org/10.1515%2Fnanoph-2020-0039.

[14] Simone Raoux et al. “Phase change materials and phase change memory”. In: *MRS Bulletin* 39 (Aug. 2014), pp. 703–710. DOI: 10.1557/mrs.2014.139. URL: https://doi.org/10.1557/mrs.2014.139.

[15] Spectra Physics. *Mai Tai® One Box Ti:Sapphire Ultrafast Lasers*. URL: https://www.spectra-physics.com/en/f/mai-tai-ultrafast-laser. (accessed: 07.06.2023).

[16] GWU-Lasertechnik. *Ultrafast Harmonic Generator*. URL: https://gwu-lasertechnik.de/ultrafast-harmonic-generator. (accessed: 07.06.2023).

[17] Newport. *Manual Variable Attenuator, Ultrafast, 690 - 1040 nm*. URL: https://www.newport.com/p/VA-BB-2. (accessed: 07.06.2023).

[18] V A Trofimov and Yu V Rublev. “DEMONSTRATION OF THE MALUS LAW”. In: *Soviet Physics Uspekhi* 11.2 (Feb. 1968), p. 276. DOI: 10.1070/PU1968v011n02ABEH003820. URL: https://dx.doi.org/10.1070/PU1968v011n02ABEH003820.

[19] Thorlabs. *PAF-X-15-PC-B - FiberPort, FC/PC, f=15.4 mm, 600 - 1050 nm, Ø3.33 mm Waist*. URL: https://www.thorlabs.com/thorProduct.cfm?partNumber=PAF-X-15-PC-B#ad-image-0. (accessed: 12.06.2023).

[20] Thorlabs. *AC254-075-B-ML - f=75 mm, Ø1" Achromatic Doublet, SM1-Threaded Mount, ARC: 650-1050 nm*. URL: https://www.thorlabs.com/thorProduct.cfm?partNumber=AC254-075-B-ML. (accessed: 11.06.2023).

[21] Thorlabs. *AC254-200-B-ML - f=200 mm, Ø1" Achromatic Doublet, SM1-Threaded Mount, ARC: 650-1050 nm*. URL: https://www.thorlabs.com/thorproduct.cfm?partnumber=AC254-200-B-ML. (accessed: 11.06.2023).

[22] Thorlabs. *PF10-03-P01 - Ø1" Protected Silver Mirror*. URL: https://www.thorlabs.us/thorProduct.cfm?partNumber=PF10-03-P01. (accessed: 12.06.2023).

[23] Thorlabs. *GL10-B - Mounted Glan-Laser Polarizer, Ø10 mm CA, AR Coating: 650 - 1050 nm*. URL: https://www.thorlabs.de/thorproduct.cfm?partnumber=GL10-B. (accessed: 11.07.2023).

[24] Thorlabs. *Cage System Construction*. URL: https://www.thorlabs.com/navigation.cfm?guide_id=2255. (accessed: 11.06.2023).

[25] Niklas Hesse. "Out of plane laser switching of chalcogenide phase change materials". University of Münster, 2021.

[26] Björn Luig. "Free-space optical control of phase-change materials in photonic circuits". University of Münster, 2023.

[27] Robert Schneider. "Aufbau eines Laser Scanning Mikroskops". University Technology Chemnitz, 2012.

[28] Thorlabs. *PAF2P-15B - FiberPort, FC/PC, f=15.3 mm, 600 - 1050 nm, Ø3.33 mm Waist*. URL: https://www.thorlabs.com/thorproduct.cfm?partnumber=PAF2P-15B. (accessed: 12.06.2023).

[29] Thorlabs. *BS014 - 50:50 Non-Polarizing Beamsplitter Cube, 700 - 1100 nm*. URL: https://www.thorlabs.de/thorproduct.cfm?partnumber=BS014. (accessed: 12.07.2023).

[30] Thorlabs. *BT620/M - Beam Trap, 1 - 12 µm, 50 W Max Avg. Power, Pulsed and CW, M4 Tap*. URL: https://www.thorlabs.de/thorproduct.cfm?partnumber=BT620/M. (accessed: 12.06.2023).

[31] Thorlabs. *GVS002 - 2D Galvo System, Silver-Coated Mirrors, PSU Not Included*. URL: https://www.thorlabs.us/thorProduct.cfm?partNumber=GVS002. (accessed: 11.06.2023).

[32] Thorlabs. *GPS011-EC - 1D or 2D Galvo System Linear Power Supply, 230 VAC*. URL: https://www.thorlabs.com/thorproduct.cfm?partnumber=GPS011-EC. (accessed: 12.06.2023).

[33] National Instruments. *BNC-2090A*. URL: https://www.ni.com/de-de/support/model.bnc-2090a.html. (accessed: 12.06.2023).

[34] Mitutoyo. *M Plan Apo NIR HR 50X*. URL: https://shop.mitutoyo.de/web/mitutoyo/de_DE/mitutoyo/05.04.05/M%20Plan%20Apo%20NIR%20HR%2050X/$catalogue/mitutoyoData/PR/378-863-5/index.xhtml. (accessed: 11.06.2023).

[35] Edmund optics. *10X EO M Plan Apo Long Working Distance Infinity Corrected*. URL: https://www.edmundoptics.com/p/10x-eo-m-plan-apo-long-working-distance-infinity-corrected/16535. (accessed: 11.07.2023).

[36] Thorlabs. *LJ1516RM-B - f=1000.0 mm, Ø1", N-BK7 Mounted Plano-Convex Round Cyl Lens, ARC: 650 - 1050 nm*. URL: https://www.thorlabs.com/thorproduct.cfm?partnumber=LJ1516RM-B. (accessed: 11.06.2023).

[37] Thorlabs. *LK1487RM-B - f=-400.0 mm, Ø1", N-BK7 Mounted Plano-Concave Round Cyl Lens, ARC: 650 - 1050 nm*. URL: https://www.thorlabs.com/thorproduct.cfm?partnumber=LK1487RM-B. (accessed: 11.06.2023).

[38] Thorlabs. *BS029 - 90:10 (R:T) Non-Polarizing Beamsplitter Cube, 700 - 1100 nm, 1"*. URL: https://www.thorlabs.com/thorProduct.cfm?partNumber=BS029&. (accessed: 12.06.2023).

[39] Thorlabs. *AC254-100-A-ML - f=100 mm, Ø1." Achromatic Doublet, SM1-Threaded Mount, ARC: 400-700 nm*. URL: https://www.thorlabs.com/thorProduct.cfm?partNumber=AC254-100-A-ML. (accessed: 12.07.2023).

[40] Thorlabs. *DCC1545M - USB 2.0 CMOS Camera, 1280 x 1024, Monochrome Sensor*. URL: https://www.thorlabs.com/thorProduct.cfm?partNumber=DCC1545M&. (accessed: 12.06.2023).

[41] Thorlabs. *AC254-075-A-ML - f=75 mm, Ø1" Achromatic Doublet, SM1-Threaded Mount, ARC: 400-700 nm*. URL: https://www.thorlabs.com/thorProduct.cfm?partNumber=AC254-075-A-ML. (accessed: 12.07.2023).

[42] Thorlabs. *ID25Z/M - Mounted Zero-Aperture Iris, Ø25.0 mm Max Aperture, TR75/M Post*. URL: https://www.thorlabs.com/thorProduct.cfm?partNumber=ID25Z/M. (accessed: 12.06.2023).

[43] Thorlabs. *S132C - Slim Photodiode Power Sensor, Ge, 700 - 1800 nm, 5 nW - 5 mW, Up to 500 mW with Filter*. URL: https://www.thorlabs.us/thorProduct.cfm?partNumber=S132C. (accessed: .06.2023).

[44] Thorlabs. *PM100D - Compact Power and Energy Meter Console, Digital 4" LCD*. URL: https://www.thorlabs.com/thorproduct.cfm?partnumber=PM100D. (accessed: 11.06.2023).

[45] Physik Instrumente. *P-541.2 • P-542.2 XY Piezo Stage*. URL: https://www.physikinstrumente.com/en/products/nanopositioning-piezo-flexure-stages/xy-piezo-flexure-stages/p-5412-p-5422-xy-piezo-stage-201530/#specification. (accessed: 12.06.2023).

[46] Physik Instrumente. *E-727.x • E-727.xAP Digital Multi-Channel Piezo Controller*. URL: https://www.physikinstrumente.com/en/products/controllers-and-drivers/nanopositioning-piezo-controllers/e-727x-e-727xp-digital-multi-channel-piezo-controller-412418442/. (accessed: 12.06.2023).

[47] Physik Instrumente. *PIMikroMove*. URL: https://www.physikinstrumente.com/en/products/software-suite/motion-control-software. (accessed: 12.06.2023).

[48] Rayleigh. *XXXI. Investigations in optics, with special reference to the spectroscope*. Aug. 1879. DOI: 10.1080/14786447908639684. URL: https://doi.org/10.1080/14786447908639684.

[49] Lin Jin. "Experimental Researches on The Amorphization of Phase Change Materials". University of Münster, 2017.

[50] R. Golovchak et al. "Oxygen incorporation into GST phase-change memory matrix". In: *Applied Surface Science* 332 (2015), pp. 533–541. ISSN: 0169-4332. DOI: https://doi.org/10.1016/j.apsusc.2015.01.203. URL: https://www.sciencedirect.com/science/article/pii/S0169433215002457.

[51] S. Privitera, E. Rimini, and R. Zonca. "Amorphous-to-crystal transition of nitrogen- and oxygen-doped Ge2Sb2Te5 films studied by in situ resistance measurements". In: *Applied Physics Letters* 85.15 (Oct. 2004), pp. 3044–3046. ISSN: 0003-6951. DOI: 10.1063/1.1805200. eprint: https://pubs.aip.org/aip/apl/article-pdf/85/15/3044/14034352/3044_1_online.pdf. URL: https://doi.org/10.1063/1.1805200.

[52] M. H. Jang et al. "Phase change behavior in oxygen-incorporated Ge2Sb2Te5 films". In: *Applied Physics Letters* 95.1 (July 2009), p. 012102. ISSN: 0003-6951. DOI: 10.1063/1.3168551. eprint: https://pubs.aip.org/aip/apl/article-pdf/doi/10.1063/1.3168551/13953620/012102_1_online.pdf. URL: https://doi.org/10.1063/1.3168551.

[53] S. M. Wiggins, J. Solis, and C. N. Afonso. "Influence of pulse duration on the amorphization of GeSb thin films under ultrashort laser pulses". In: *Applied Physics Letters* 84.22 (May 2004), pp. 4445–4447. ISSN: 0003-6951. DOI: 10.1063/1.1759062. eprint: https://pubs.aip.org/aip/apl/article-pdf/84/22/4445/10203598/4445_1_online.pdf. URL: https://doi.org/10.1063/1.1759062.